CHAPTER

8

Fault classification, fault growth and displacement

Haakon Fossen

Museum of Natural History/Department of Earth Science, University of Bergen, Bergen, Norway

Introduction

Predicting fault locations and fault properties such as geometry, horizontal and vertical length, connectivity and displacement has been important to the mining industry for many centuries because of the ability of faults to conduct fluids and therefore host ore deposits, and for their tendency to complicate mining operations, particularly coal mining. More recently, it has become essential to understand faulting and to predict fault locations, geometries, orientations and properties in the context of oil and gas exploration and exploitation. As a consequence, much of our current understanding of faults is based on research driven by industrial needs, particularly since the 1980s when three-dimensional (3D) reflection seismic data sets became available. Since then we have seen an impressive improvement in seismic data quality and data enhancement methods that, together with field-based studies and physical and numerical modeling, has led us to the current understanding of faults and faulting. At a larger scale ($>1-10$ km) than that concerning hydrocarbon production and most mining operations, faults or fault zones affect the entire brittle crust and link with deeper lithospheric shear zones and may generate devastating earthquakes during their active lifetime. However, they all initiate as small features and grow into larger faults, fault zones and fault networks. The process by which faults form and grow and the related complications and fault geometries are the main focus of this chapter. This review is largely presented in the context of the normal fault regime, but most principles and properties apply also to strike-slip and thrust settings.

What is a fault?

A fault represents a narrow physical discontinuity in rock and in the displacement field associated with the deformation, exhibiting predominantly shear (wall-parallel) displacement. Small-scale structures (e.g. magnified part of Fig. 8.1A) that fit this definition are usually referred to as shear fractures, while a fully developed fault is a composite structure that consists of a multitude of smaller-scale structures in a zone, together with one or more major slip surfaces and/or a fault core along which most of the offset is localized. Hence faults as observed in outcrop are rarely simple discrete "planes", but rather irregular curvitabular volumes of variably deformed rocks. Typical elements found in such volumes are subsidiary faults, fractures, veins, gouge, breccia, deformation bands and volumes or lenses of less- or undeformed host rock. Large faults are well known to consist of multiple smaller fault elements in a zone (e.g. Braathen et al., 2009); hence, the term *fault zone* has for a long time been used to emphasize the fact that large faults are composite structures consisting of a multitude of smaller-scale faults and associated structures (Caine et al., 1996; Childs et al., 1996; Wibberley et al., 2008; Wibberley and Shipton, 2010).

Regional Geology and Tectonics.
DOI: https://doi.org/10.1016/B978-0-444-64134-2.00007-9

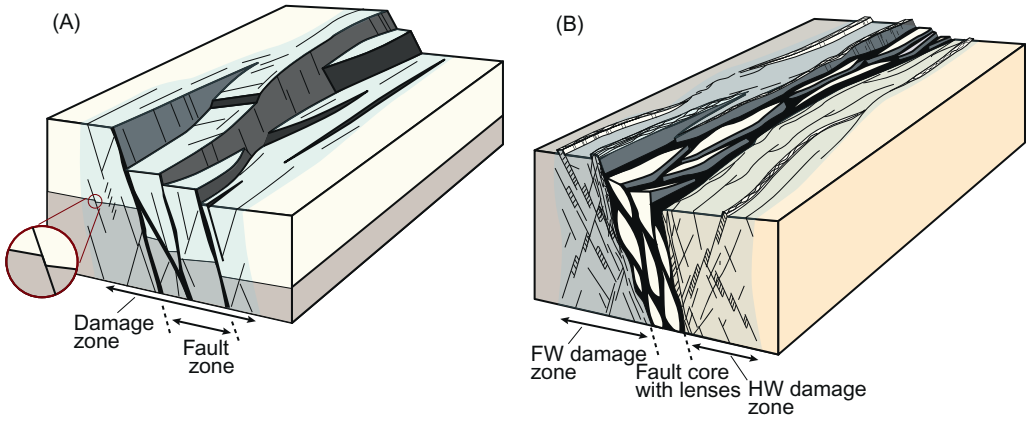

FIGURE 8.1 Conceptualized illustrations of a complete fault and its different elements. (A) Slip localized on two or more narrow high-strain zones (slip surfaces or fault cores shown in black). A subsidiary footwall shear fracture is highlighted. (B) High-displacement fault showing a more extensively sheared central core with a surrounding low-strain damage zone. Source: *(A) Figure inspired by Childs, C., Nicol, A., Walsh, J.J., Watterson, J., 1996. Growth of vertically segmented normal faults. J. Struct. Geol. 18, 1389–1397.*

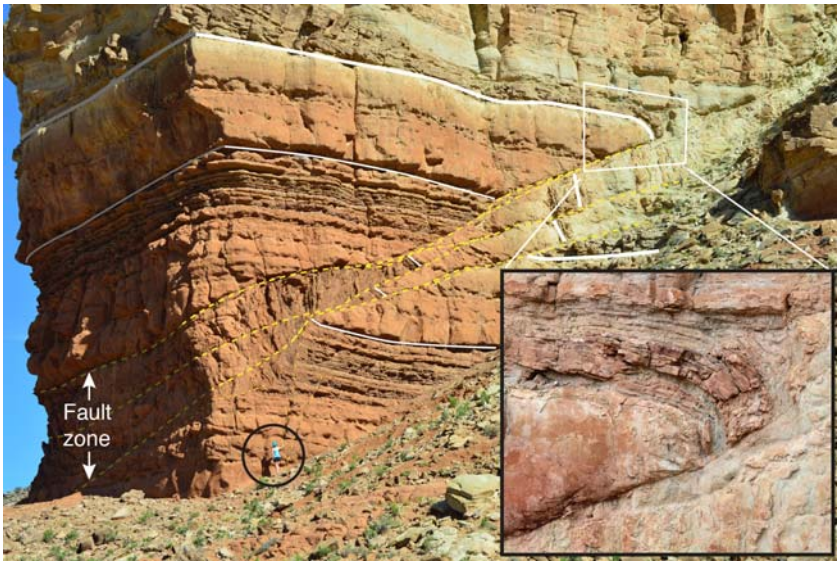

FIGURE 8.2 Example of a fault zone (reverse) in the Entrada Sandstone, Southern Utah. Rotation of layering in the zone and local normal drag along the bounding faults can be interpreted as evidence for breaching of a fault-propagation fold.

Fault anatomy

The term fault zone is also used for smaller (outcrop-scale) faults that display composite structural elements, particularly where several slip surfaces can be discerned (Childs et al., 1996; 2009; Wibberley et al., 2008) (Fig. 8.1A). An example of a typical fault zone of this kind is shown in Fig. 8.2, where several closely arranged slip surfaces in a reverse fault zone have accommodated shortening of the Jurassic Entrada Sandstone in the Sevier foreland, Utah. The internal anatomy of many faults or fault zones fits the simple twofold classification of a central fault core and an enveloping damage zone (Caine et al., 1996) (Fig. 8.1B). Here, the *fault core* consists of highly sheared rocks that may be represented by fault gouge, cataclasite or breccia in which the original structure of the rock has been strongly masked or destroyed (Fig. 8.3). Its nature depends on the rocks involved; shale would easily create a zone of clay smear, while limestone, sandstone and igneous rocks typically develop different kinds of cataclasites and breccias. Large faults that have experienced late reactivation at shallow crustal levels may show a central core of noncohesive material within a more cohesive cataclastic outer core that formed during fault motions at greater depth (Fig. 8.3C). Variably deformed lenses of the wall rocks may form an integral part of the fault core (Fig. 8.1B), or when above a certain size, may be considered as a separate architectural element of a fault.

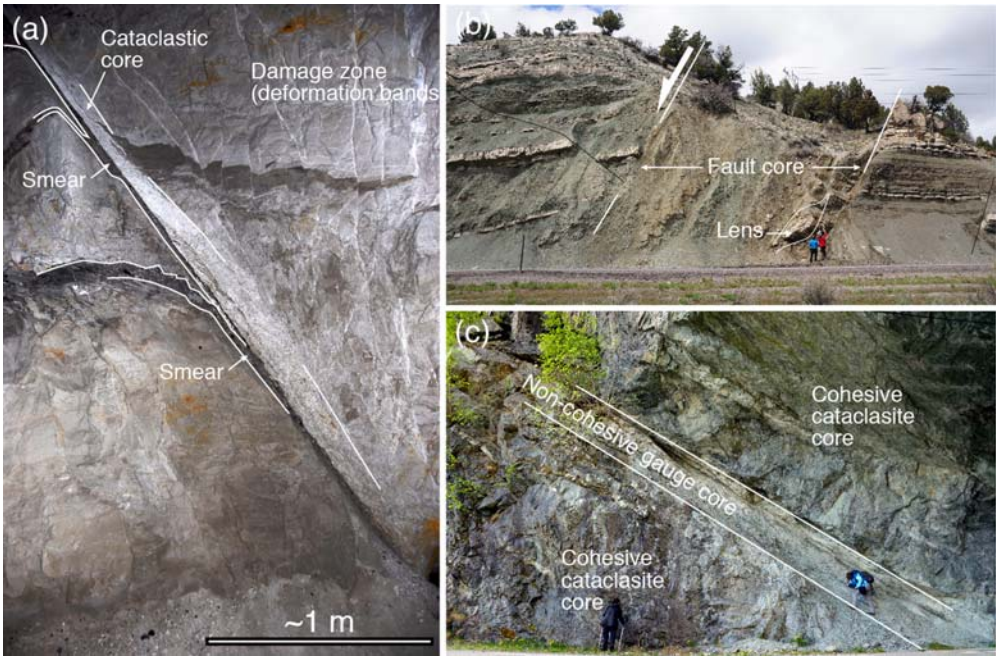

FIGURE 8.3 Three examples of fault cores in different lithologies. (A) Fault core with damage zone developed in Cretaceous fluvial sediments (near Salina, Utah, ca. 20 m offset). The core consists of crushed sandstone (cataclastic) and smeared clay-coal layers. (B) Fault with ~100 m offset developed in shales of the Green River Formation, Utah. (C) Central noncohesive fault core surrounded by older flinty cataclasite as part of a several hundred meters–wide fault core in metamorphic rocks. Lærdal-Gjende fault, Norway, with several kilometers offset.

In the fault core-damage zone terminology, a fault core is completely surrounded by the *damage zone*, which is a zone of relatively low-displacement structures, notably shear fractures, but also veins (mineral filled extension fractures), short joints, deformation bands and/or stylolites (Fig. 8.1). Large faults may also contain smaller faults with their own damage zones, contained within the large damage zone of the first-order fault, as shown schematically in Fig. 8.4. Hence, the definition of a damage zone is to some extent scale-dependent. The relationship between fault displacement and damage zone width, however, seems to be rather scale-independent over a large range of sizes, meaning that the ratio between damage zone width and displacement is statistically the same for small and large faults. This emerges from plots such as the one shown in Fig. 8.5, which suggests a thickness–displacement ratio of 1:100 (displacement being 100 times the damage zone thickness). Note however that more specific data sets may deviate from this global rule (e.g. data from porous sandstones; Schueller et al., 2013), so establishing a relationship for specific areas and parts of the stratigraphy is always recommended. The scatter is also very large. Therefore, estimating displacement from damage zone thickness involves a large uncertainty. Field observations also show that damage zone width can vary greatly both vertically and laterally along a single fault due to variations in lithology, fault geometry and growth/linkage history. Fault core data from a variety of fault sizes also show a general increase in fault core thickness with increasing fault displacement, but with a similar two orders of magnitude uncertainty (Fig. 8.5).

The anatomy of damage zones is also of interest, and their inner part generally contains a higher density of small-scale structures than do their peripheral part. An inner damage zone with higher density of structures and more complex structural relations can sometimes be distinguished from an outer low-strain damage zone (e.g. Cerveny et al., 2004; Berg and Skar, 2005). However, statistical evaluation of damage zones from extensional faults in porous sandstones (Schueller et al., 2013) has shown that most faults show a gradual decay in deformation band frequency away from the fault core, and that statistically this decrease can be described as logarithmic. Schueller et al. (2013) also suggest a scale-invariant growth process where the average density of deformation bands (15 ± 9 bands/m) is statistically independent of fault displacement. Further, the distribution of deformation bands within the damage zone is qualitatively similar for small and large faults. Fault damage zones in nonporous or low-porosity rocks show a similar decay in fracture density away from the fault core (e.g. Caine et al., 1996; Faulkner et al., 2011). Furthermore, Savage and Brodsky (2011) suggested that the fracture density decay inside damage zones can be described by a power law with an average decay rate of approximately 0.8. Johri et al. (2014) numerically modelled

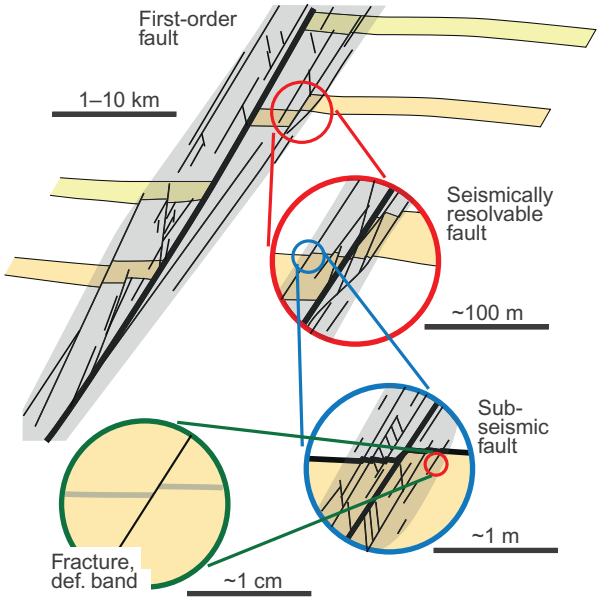

FIGURE 8.4 Schematic illustration of fault hierarchy, from major first-order fault with several kilometers of displacement down to the scale of individual fractures or deformation bands. Three orders of damage zones are indicated, observable at different scales.

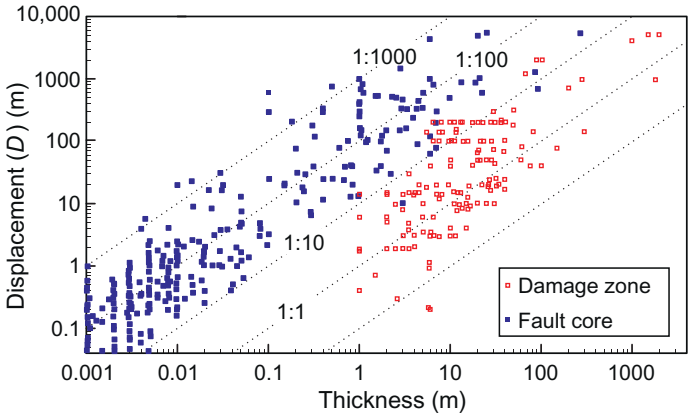

FIGURE 8.5 Fault displacement plotted against fault core and damage zone thickness in logarithmic diagram. Note that the fault core is on average two orders of magnitude thinner than the damage zone. Source: *Modified from Fossen, H., 2016. Structural Geology, second ed. Cambridge University Press, Cambridge.*

such a power-law decrease in fracture intensity away from the fault core. However, many such data sets are extracted from small faults with meter-scale displacement or less and do not reflect the complexity and variations associated with fault damage zones in nonporous rocks in general.

Fault drag

The zone of fault-related folding along many faults, known as *drag folding*, is not considered as part of the fault itself, but nevertheless adds to its total displacement. Drag develops where a layering is oriented at an angle to the slip vector of the fault, for example horizontal beds affected by a normal or reverse fault. The term normal drag (normal in the sense of being common) is used about markers that are convex in the direction of slip. Similarly, reverse drag applies where markers are concave in the direction of slip (Grasemann et al., 2005). In other words, drag is considered to be normal when rotated into the fault (zone) in the same way that layers in

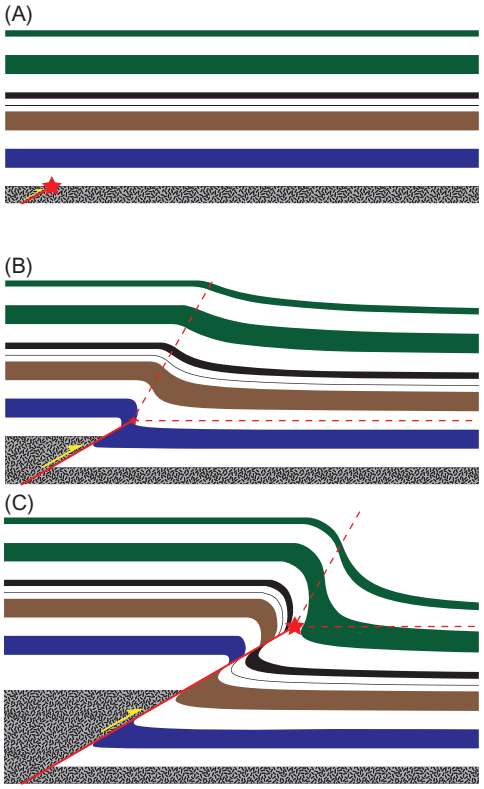

FIGURE 8.6 Formation of normal drag associated with a reverse fold as a result of fault-propagation folding. The fold forms ahead of the propagating fault tip (a-b) and is at some point dissected by the fault (lower part of B and C). Trishear modeling (Erslev, 1991). Source: *Modified from Fossen, H., 2016. Structural Geology, second ed. Cambridge University Press, Cambridge.*

metamorphic rocks are rotated into ductile shear zones (Ramsay, 1980). Note that normal and reverse drag are merely geometrically descriptive terms, so that both normal and reverse drag can be associated with normal faults, for example. Also note that normal drag along a reverse fault is geometrically similar to reverse drag along a normal fault. For instance, the drag along the reverse faults in Figs 8.2 and 8.6 is normal, while the km-scale drag related to the large normal fault in Fig. 8.7 is reverse. Also note that there is normal drag in a narrow zone along the main fault in the Jurassic section in Fig. 8.7.

The drag zone can vary from less than a meter to several kilometers in width (Fig. 8.7) and typically varies vertically as layers of different mechanical properties get involved, but also laterally in many cases. In general, shales and clay-rich sequences tend to develop drag more easily than massive competent units (well-lithified sandstones and limestones). Drag zones that are wide enough to be imaged on seismic data are typically wider in the hanging wall than in the footwall.

Drag may have several causes (Grasemann et al., 2005) and should only be used as a descriptive term about fault-adjacent layer rotation (folding). While friction along the fault core was typically called for in the older literature, *fault-propagation folding* is now considered to be a more common drag-forming mechanism. In the fault-propagation model, for which there is abundant evidence from many field examples, physical experiments and numerical models, a precursory fold forms by distributed deformation ahead of the propagating fault tip, and the fold becomes a drag fold the moment the tip propagates through the fold (Fig. 8.6). Impressive examples of Laramide-age fault-propagation monoclines underlain or cut by upward propagating basement faults are exposed on the Colorado Plateau (e.g. Zuluaga et al., 2014). Drag folds can also form along an existing fault due to fault bends and geometric complications caused by fault linkage processes. Because these complications tend to vary rapidly both laterally and vertically along faults, so does the appearance of drag. Rollover folds are a special case of reverse drag explained by listric normal fault geometry and are typically much larger than many other types of drag folds. Finally, differential compaction across major faults can also produce or add to large-scale drag geometries. Drag folds are particularly important in hydrocarbon reservoirs where drag can significantly change the communication pattern across faults.

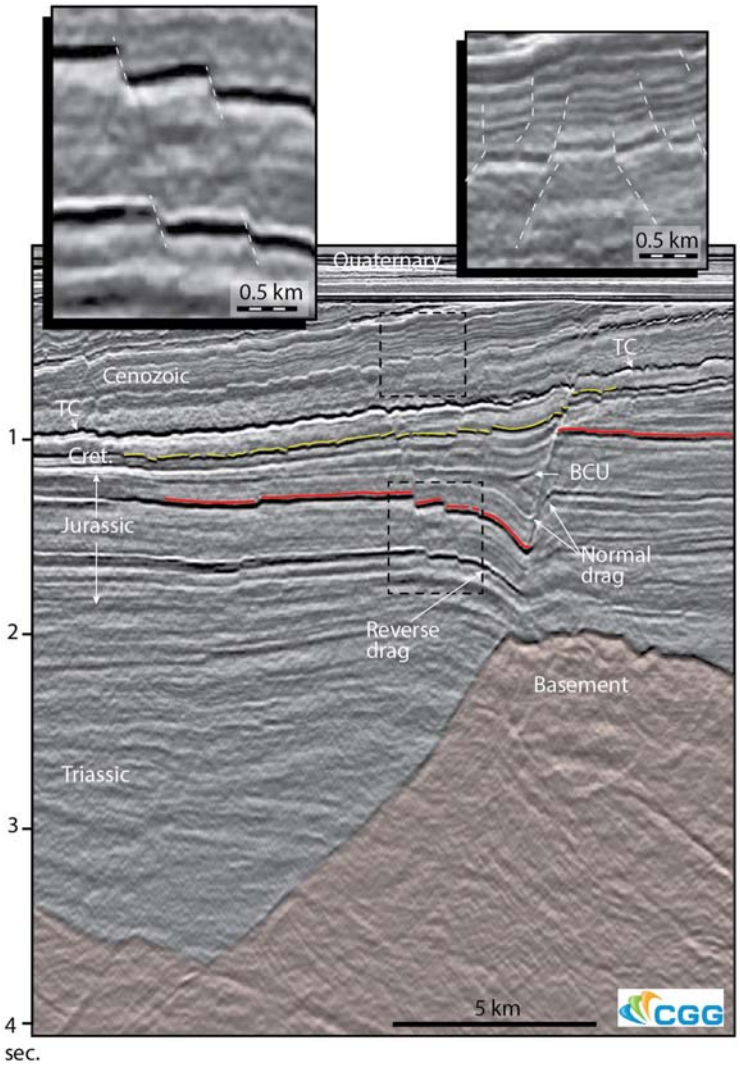

FIGURE 8.7 Example from the northern North Sea rift of how faults of different sizes typically appear on reflection seismic sections. The main fault offsets the rift basement by several kilometers, while its offset through the Jurassic section is only a few hundred meters, reducing to less than a hundred meters at the top Cretaceous (TC) level. Smaller antithetic faults in the hanging wall are magnified (upper left), as are nontectonic faults in the Cenozoic post-rift package (upper right). These shallow faults are related to sediment compaction and dewatering. The magnified images show that there is room for different fault interpretations, with a zone of uncertainty of at least 100 m in width in this particular example that contains the fault damage zone and potential fault complications. Examples of normal and reverse drag are indicated. BCU, Base Cretaceous Unconformity. Source: *Seismic data, courtesy of CGG.*

Fault orientations, stress, strain and kinematics

Relation between faults and stress

Faults initiate with orientations that are largely controlled by the orientations of the principal stretching directions, which for structures involving small offsets and negligible block rotations can be correlated with principal stress directions (σ_1, σ_2, σ_3). A simple relationship between stress and faults for isotropic rocks was used by Anderson (1951) as he defined his three tectonic regimes: normal, thrust and strike-slip (Fig. 8.8). Using the Coulomb criterion and a coefficient of friction of 0.6 (typically taken to be representative for common rock types, Byerlee's Law) an angle of 30 degrees can be predicted between the maximum compressive stress (σ_1) or shortening direction and the fault. This means that normal faults ($\sigma_1 = \sigma_v$) can be expected to dip at around 60 degrees, while reverse faults dip at around 30 degrees ($\sigma_1 = \sigma_H$), unless guided by preexisting structures. Strike-slip faults on the other hand are predicted to be vertical in this scheme.

The simple Andersonian plane-strain model for faulting shown in Fig. 8.8 is founded on the assumption that the three principal stresses are always vertical or horizontal. In nature many, if not most, faults show evidence of oblique-slip, with components of both strike-slip and dip-slip displacement. Important reasons for this rotation of the principal stress axes are stress perturbations caused by mechanical strength variations, notably around weak faults and fractures, by slip along nonplanar faults, by slip along foliations, by rock anisotropy in general and by fault interaction in both the horizontal and vertical directions.

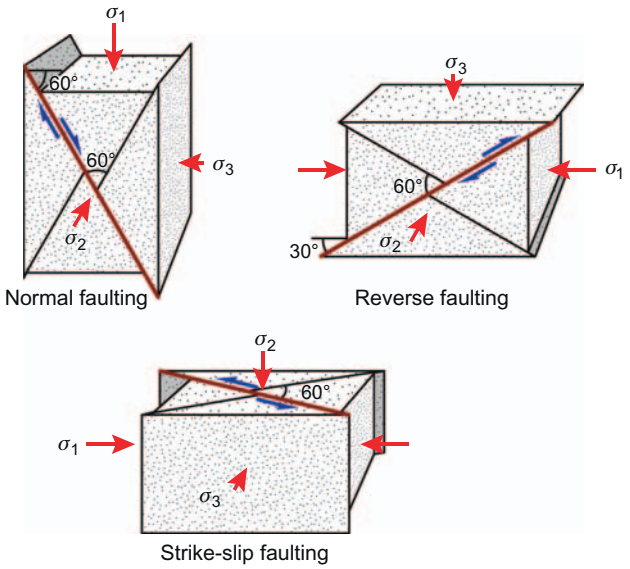

FIGURE 8.8 Relation between the principal stress orientations and faults in the three Andersonian regimes, as illustrated by conjugate fault sets. These idealized figures show a close relationship between principal stress (or strain) axes and conjugate faults. Principal stress axes are indicated, but note that strictly speaking, these axes are instantaneous strain axes. Source: *Modified from Fossen, H. 2016. Structural Geology, second ed. Cambridge University Press, Cambridge.*

In naturally deformed rocks, the orientation of the principal stresses is well constrained where faults form two conjugate sets with opposite shear sense. Conjugate in this sense implies that the two sets were active at the same time, so that they locally or in a limited region show mutual crosscutting relationships. In this case, the shortening direction bisects the acute angle between the two sets of shear structures and can, for small displacements, be interpreted to represent σ_1. Consequently, σ_2 parallels their line of intersection, and σ_3 bisects the obtuse angle between the shear structures, as shown in Fig. 8.8.

Where fault slip data (fault orientation and direction and sense of slip, and if possible, amount of displacement) can be collected for a local fault population, paleostress or strain axes can be estimated by means of stress inversion methods (Angelier, 1979, 1984; Etchecopar et al., 1981) or kinematic analysis (Marrett and Allmendinger, 1990). Stress inversion analyses are based on the Wallace–Bott hypothesis, which makes the assumption that slip on a surface will occur in the direction of maximum resolved shear stress. Applying this hypothesis to measured fault slip data enables us to estimate the orientations of the principal stresses (Angelier, 1994). However, it can be argued that any fault analysis that is based on measurements of slip surfaces, slip directions and sense of slip are, strictly speaking, a kinematic approach that primarily gives the principal shortening (P) and extension (T) axes, as outlined by Marrett and Allmendinger (1990), and that stress can only be indirectly correlated with these axes, assuming no rotation of structures during deformation.

Strain and fault orientation patterns

Simple conjugate sets of faults are compatible with plane strain, where the length of the intermediate strain axis Y remains unchanged during deformation. For the normal fault regime, the horizontal extension direction is then perpendicular to the (average) strike of the faults, and for a thrust belt setting, the principal horizontal shortening direction is perpendicular to the strike of the faults. Both natural fault populations and those formed during physical and numerical experiments show some variation in strike direction. Plane-strain experiments show such variations very well (Fig. 8.9B and C), and there are many examples of natural fault populations at different scales that contain faults or fault segments at low angles to the extension or shortening direction (e.g. Fig. 8.9A). In detail, we usually find fault bends and segments of somewhat different orientations, and zigzag-like geometries also occur in both numerical models (Cowie et al., 2000; Finch and Gawthorpe, 2017; Deng et al., 2017) and in nature.

Two or more double sets of conjugate faults can also result from a single deformation episode, reflecting 3D (or triaxial) strain of the flattening type with extension along two principal strain axes (X and Y) (Oertel, 1965; Krantz, 1988; Reches, 1988; Healy et al., 2015) (Fig. 8.10) or doming with shortening in two directions. Hence,

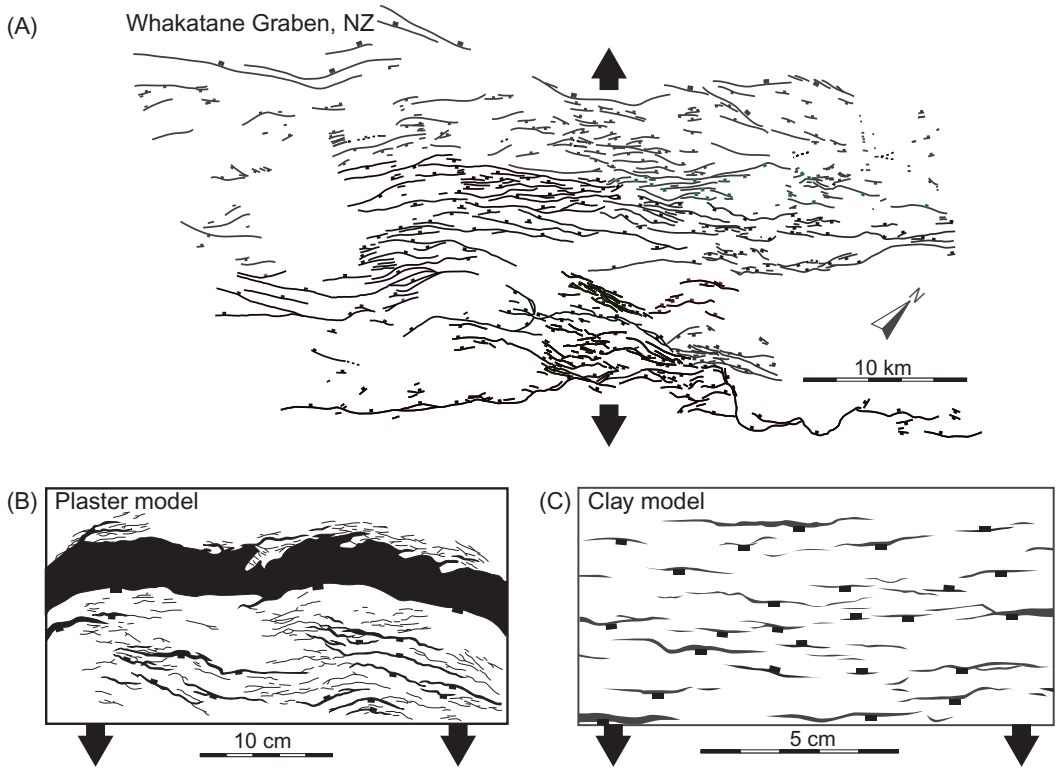

FIGURE 8.9 Fault populations formed under approximate plane-strain conditions. (A) Whakatane Graben, New Zealand. This graben has been interpreted to have a slight transtensional character, but is close to pure extension. (B) Plaster model. (C) Detailed view of clay model. In all the models the faults trend nearly perpendicular to the extension direction. Some local variations in strike orientation can be related in most cases to their growth history. Source: *(A) Modified from Lamarche, G., Barnes, P.M. Bull, J.M., 2006. Faulting and extension rate over the last 20,000 years in the offshore Whakatane Graben, New Zealand continental shelf. Tectonics, 25. doi:10.1029/2005tc001886. (B) Redrawn from Blækkan, I., 2016. Evolution of normal faults and fault-related damage: insights from physical experiments, Master thesis, University of Bergen. 86 pp. (C) redrawn from picture in Ackermann, R.V., Schlische, R.W. & Withjack, M.O., 2001. The geometric and statistical evolution of normal fault systems: an experimental study of the effects of mechanical layer thickness on scaling laws. J. Struct. Geol. 23, 1803–1819.*

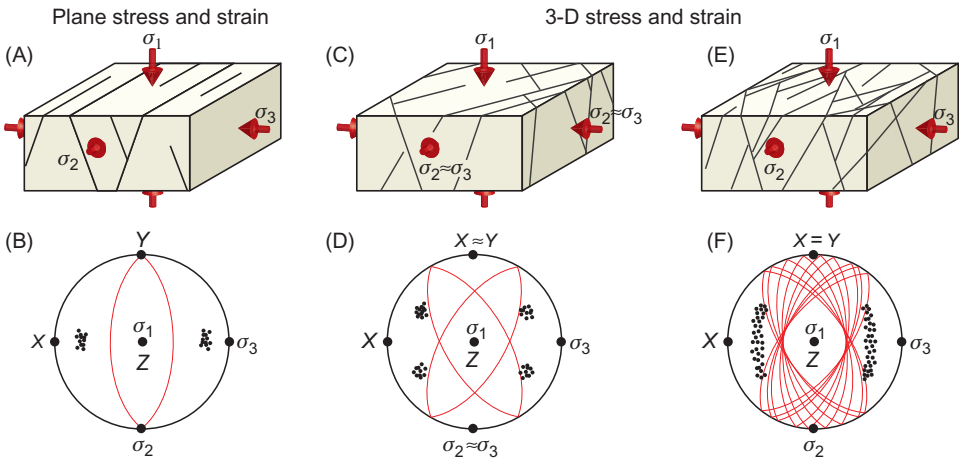

FIGURE 8.10 Idealized relationship between fault patterns and strain (or stress), shown for the normal fault regime. Simple Andersonian-style conjugate fault sets (A) result from plane strain, while orthorhombic (B) or polymodal pattern result where the resulting strain is nonplanar (i.e. 3D or triaxial strain). Figures (A, C, and D) show initial fracture pattern in relation to principal stress axes. Figures (B, D and E) show the appearance of the fractures (faults) in spherical projections and also show the strain axes ($X \geq Y \geq Z$).

3D strain of this kind results in a large variety in fault orientation caused by a single phase of deformation. This is the case where the different sets mutually crosscut each other; in contrast, if one set (orientation) systematically crosscuts another within a region, we are more likely looking at two phases or stages of deformation.

Preexisting structures have been shown to influence fault orientation to various degrees, depending on their orientation (strike and dip), size, geometry and strength (e.g. Sibson, 1985). Two general cases can be envisioned in the context of a sedimentary basin: one where a sedimentary sequence is exposed to two phases of deformation with different extension directions, and a single phase where earlier structures occur in the basement beneath the basin. The first case has been explored through physical modeling by Henza et al. (2010), who looked at changes in extension direction at up to 45 degrees. Their experiments show that the preexisting structures are obliquely reactivated together with the formation of new faults that variably cut or terminate against older faults. The result is a complex fault pattern with a large variation in fault trends. The effect of the angle between the two extension directions would vary for natural cases, depending on fault properties, length, dip and planarity, but the experiments illustrate well how composite fault patterns may emerge from two deformation phases with extension directions differing by up to 45 degrees. Further complications occur when faults are reactivated in a different tectonic regime, for instance normal faults reactivated as reverse faults (Kelly et al., 1999; Marshak et al., 2000; Zuluaga et al., 2014). For instance, reverse faults preferentially form at a lower dip angle than normal faults (Fig. 8.8) and may utilize preexisting normal faults to a lesser extent, forming hanging-wall shortcuts in their upper parts (e.g. Amilibia et al., 2008).

The second case, where an undeformed sedimentary sequence overlies a basement with preexisting structures, reactivation and upward propagation of basement faults can occur. Again, reactivation is highly dependent on orientation, geometry and strength of the preexisting basement structures. The strength of a preexisting shear zone or fault core in metamorphic basement rocks is difficult to predict and would also vary laterally and vertically. There are many examples where basement structures are reactivated in contraction, strike-slip and extension (e.g. Bailey et al., 2005; Bird et al., 2015; Phillips et al., 2016; Peace et al., 2018). In general, reactivation of basement structures involves a combination of upward propagation of the basement fault and nucleation of new faults above the basement structure that may link up and form a composite fault zone as strain accumulates (see section 'Fault Growth' below). Fault-propagation folding commonly occurs in the overlying sedimentary sequence during basement fault reactivation, both in extensional (Sharp et al., 2000) and contractional (Zuluaga et al., 2014) settings.

Displacement distributions on faults

Isolated faults tend to show a gradual increase in displacement from the tipline towards a central point, and ideally the tipline is more or less elliptical, as shown in Fig. 8.11. This simple elliptical pattern of displacement contours is modified in mechanically stratified rocks. For horizontal layering, the elliptical shape is replaced by a more rectangular shape because of the vertical growth restriction imposed by the layering. For example, a close to circular tipline may be established as a fault initiates in a strong layer (Fig. 8.12A), but ellipticity changes dramatically when the radially propagating fault reaches the top and bottom of the strong layer: the layer boundaries impose restrictions on fault tip propagation (Fig. 8.12B). At some point, the fault will break through the restricting layer boundary, and the ellipticity decreases again. Further complications arise from fault linkage, as discussed below.

Displacement profiles across faults show how displacement varies in the horizontal or vertical direction, and how the maximum displacement (D_{max}) along such profiles generally increases with fault length (or height if measured in the vertical direction). This relation has been quantified by field investigations and seismic data interpretation. Global data that span many orders of magnitude show an approximately linear relationship between fault length and displacement ($D \approx 0.3L$, Fig. 8.13). In detail, the data show a considerable spread, about 2–3 orders of magnitude, which may be due to fault growth by linkage (see below), crustal anisotropy (including layering) and 3D sampling effects. Hence, prediction of fault length from D_{max} or vice versa is possible, but only with a considerable uncertainty, unless the relationship can be better constrained for the region or stratigraphic section in question.

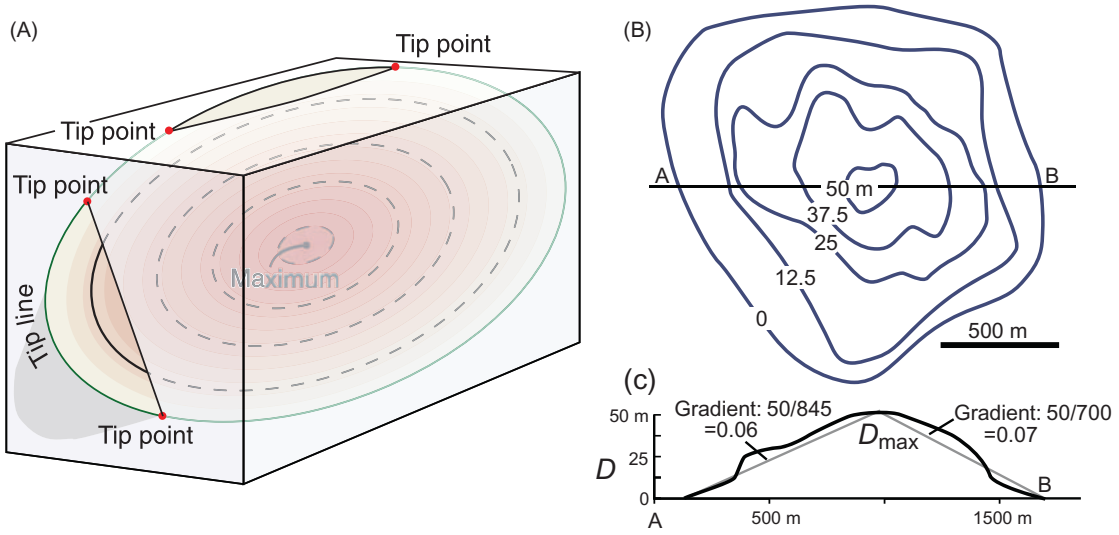

FIGURE 8.11 Displacement contours on a fault, idealized schematic model (A) and as interpreted from seismic data (B). The outer contour line (0 m) is the tipline of the fault. Figure (B) represents an isolated fault, as interpreted by Childs et al. (2003). (C) Displacement profile through the centre of the fault, with calculated average displacement gradients (0.06 and 0.07 for each side of the maximum). D – displacement.

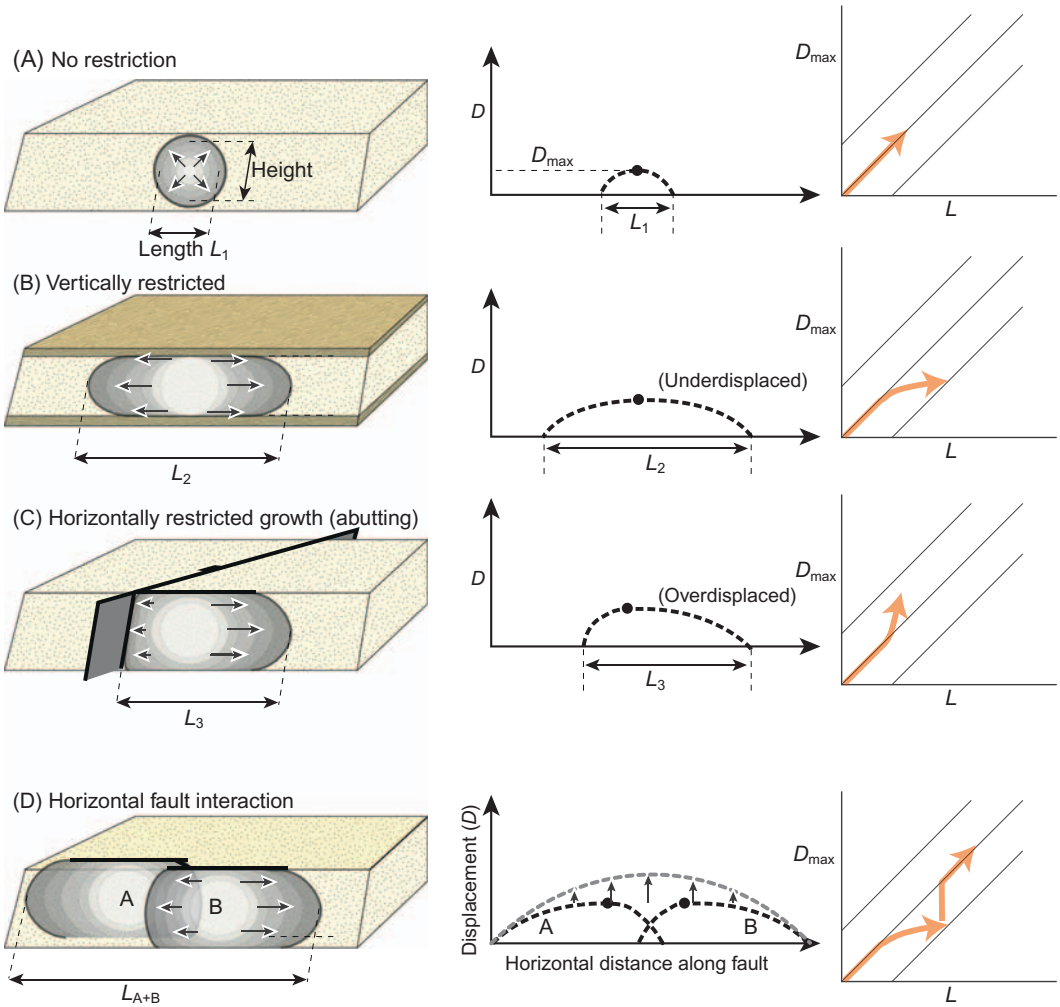

FIGURE 8.12 Schematic models of fault growth in isotropic (A), vertically restricted (B) horizontally restricted (C) and fault overlap interactive (D) settings. Also shown are displacement profiles and D_{max}-L evolution for each case. Source: *In part from Fossen, H., 2016. Structural Geology, second edition. Cambridge University Press, Cambridge.*

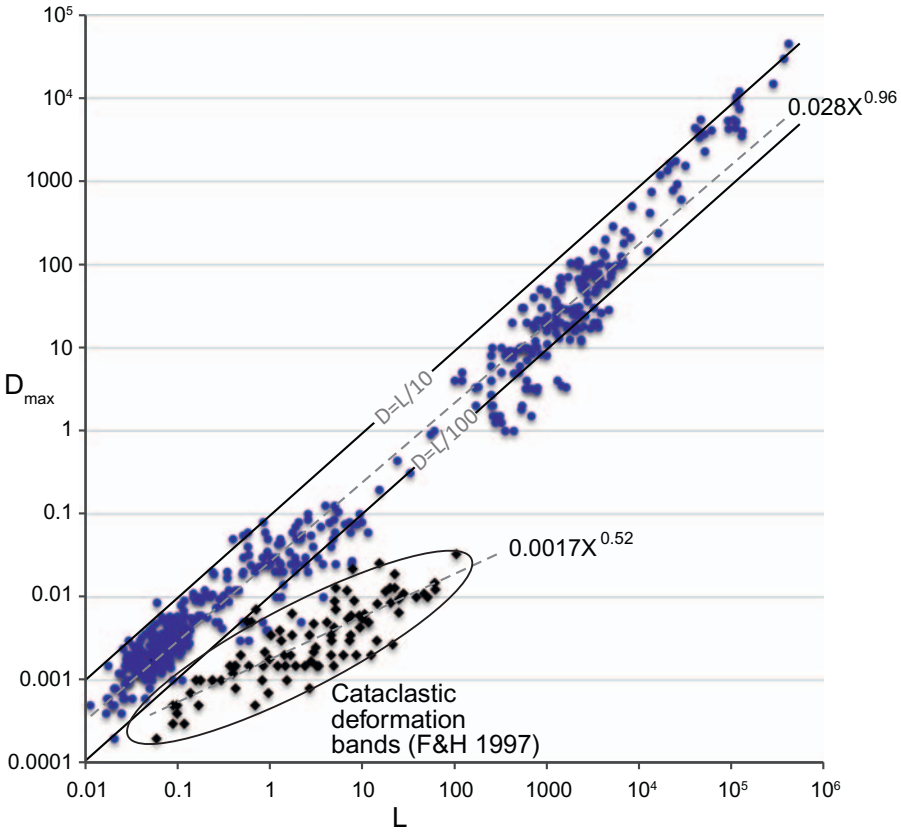

FIGURE 8.13 Maximum displacement plotted against length for faults from different settings in logarithmic diagram (mostly normal faults). Cataclastic deformation bands are shown as a separate data set. Own data + data cited in Schultz et al. (2008). F&H – Fossen & Hesthammer. Note that straight correlation lines in log-log space represent power-law scaling relations, with the slope representing the exponent. In this case, the slope (0.96) is close to 1, in which case the relation between D and L is close to linear: $D = 0.3L$. Source: *From Fossen, H. & Hesthammer, J., 1997. Geometric analysis and scaling relations of deformation bands in porous sandstone. J. Struct. Geol., 19, 1479–1493.*

Fault initiation

Fault formation from scratch

The initiation of faults in macroscopically homogeneous layers can be explored by physical modeling. Several studies demonstrate how a fault can develop from an array of minor precursor structures that define a brittle shear zone and are oriented at an angle to the initial shear zone boundaries and the resulting fault zone (Cloos, 1928; Riedel, 1929; Tchalenko, 1970). These incipient brittle structures tend to be oblique to the zone that they define, and based on their orientations and sense of slip they have been categorized into R (Riedel) and R′ (antitheric Riedel) shears. Ideally, R and R′ shears form conjugate sets that are bisected by the largest principal stress direction (σ_1). An additional set of P shears that form at low angles to the zone can also occur (Fig. 8.14A). Examples are shown in Fig. 8.14 from sandstones (B and C), plaster experiment (D) and by a recent strike-slip earthquake surface rupture pattern (E), and also in gneisses in Fig. 8.15. As displacement accumulates, these precursor structures start to connect to form a continuous fault zone rather than a simple fault "plane" (Fig. 8.14F).

In other cases, arrays of extensional en-echelon–arranged veins form (Fig. 8.16), particularly in strong rock layers. A component of ductile deformation is sometimes revealed by the rotation of the central and oldest portions of the veins, generating a sigmoidal vein geometry that at some point will be cut by new veins. Eventually, the zone will be breached, and a continuous fault zone forms (Fig. 8.15B), similar to the situation described above for R and R′ structures, and one or more continuous striated slip surfaces form (Fig. 8.15C). In carbonates, stylolites may form perpendicular to the veins (Fig. 8.16), and the orientations of vein tips and stylolites reveal the orientations of the instantaneous stretching directions (ISA), commonly equated to σ_3 and σ_1 for idealized

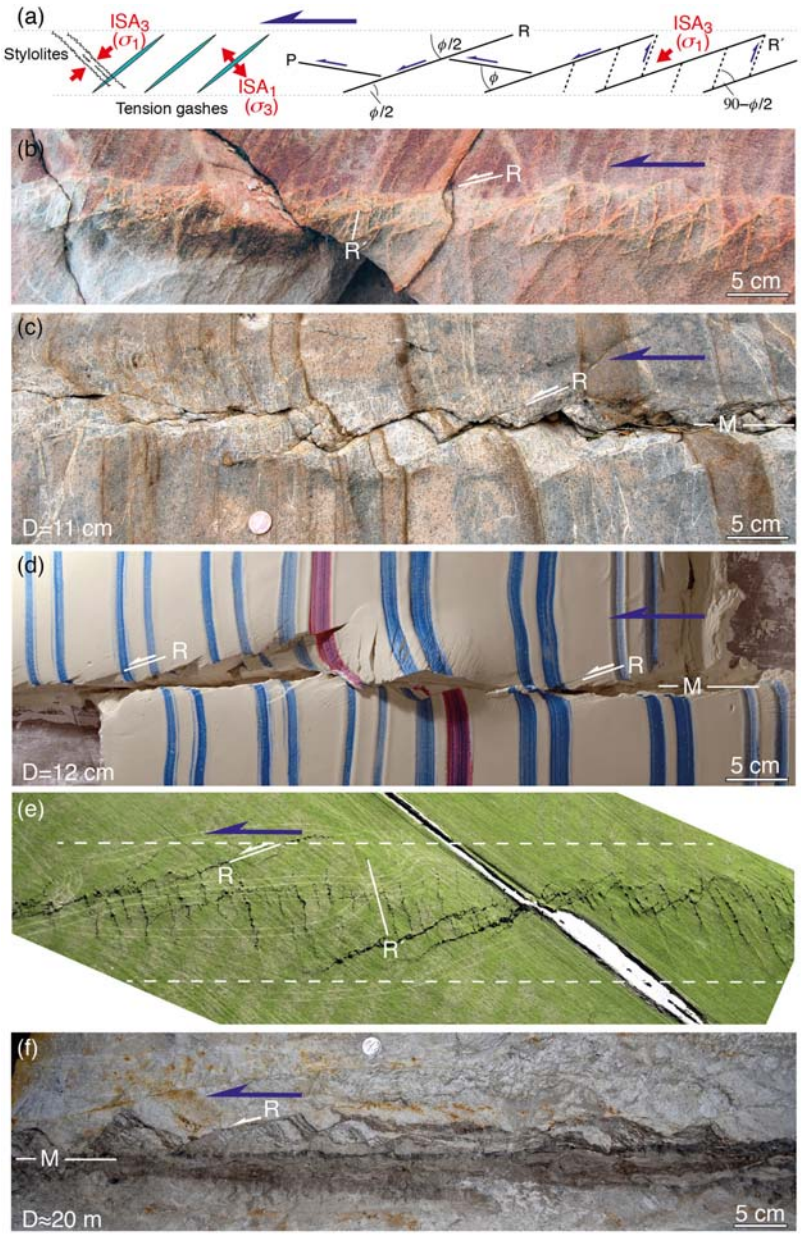

FIGURE 8.14 Early (A–E) and advanced (F) stages of faulting. (A) Principal sketch showing the orientation of different kinds of subsidiary structures: R – Riedel shears, R′ – antithetic or conjugate Riedels, P – P-shears and ISA – instantaneous stretching axes. (B–C) Ladder structures in sandstone, composed of deformation bands. (D) Plaster experiment. (E) Surface rupture pattern during the 2010 Canterbury earthquake, New Zealand. (F) Fault in sandstone showing R shears (R) adjacent to the main slip surface M. Detail from Fig. 8.3A. Source: *(E) Photo by New Zealand Ministry of Civil Defence & Emergency Management, used with permission.*

low-strain situations (Fossen, 2016). ISA_1 is the fastest stretching direction and would then correspond (by orientation, not magnitude) to σ_3. σ_1 would correspond to ISA_3, which is the slowest (usually negative) stretching direction or, in terms of shortening, the fastest shortening direction.

Most rocks are not homogeneous, but involve a metamorphic or depositional layering, which complicates fault formation and growth. In mechanically stratified sections that are exposed to layer-parallel stress, faults initiate in the stiffest or strongest layers or sequence of layers, that is layers with highest Young's modulus. These are layers where stress is concentrated, and where the rock first yields (e.g. Gudmundsson, 2011). Hence, faults initiate in several different competent layers at more or less the same time in such layered rocks.

Brittle deformation may initiate as shear fractures, extension fractures (joints, fissures or veins) or hybrid fractures. For example, turbidites, with strong sandy and sometimes calcareous layers alternating with mechanically weak shale (Fig. 8.17A), commonly show evidence of early extension fracturing and vein formation, followed by linkage as shown schematically in Fig. 8.17B–D. The different orientations of the extension structures (veins) and the resulting fault, together with any steps formed during linkage, create a zone of deformation rather than a simple slip plane.

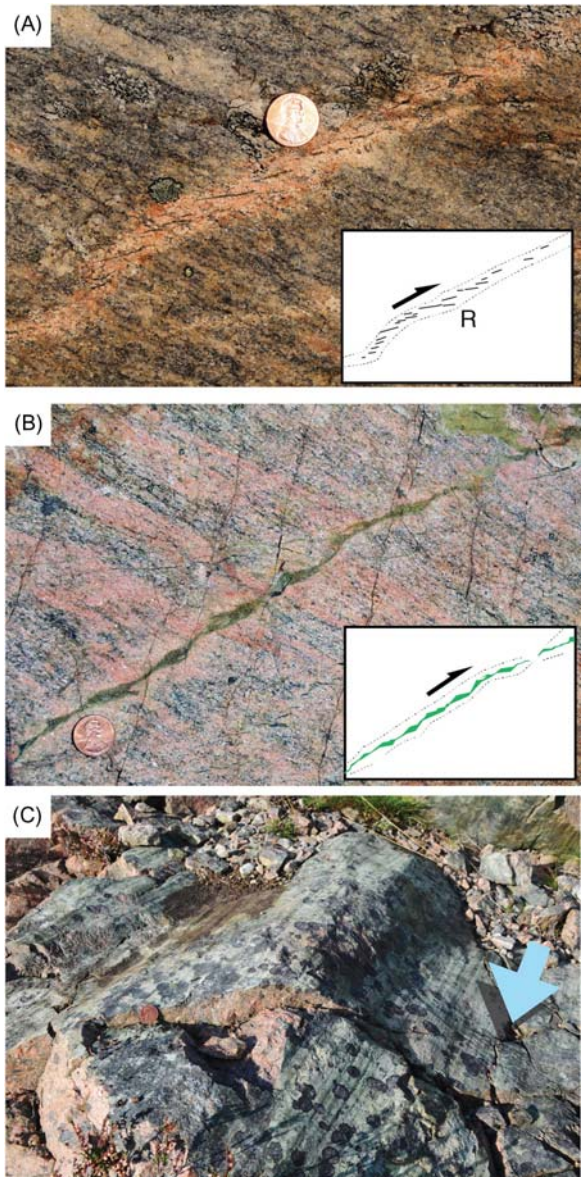

FIGURE 8.15 (A) En-echelon fractures forming during incipient stages of faulting. (B) Veins are connected and filled with epidote. (C) Further shear on the fracture/vein creates striations on a smooth but curved surface. The axis of curvature indicates the slip direction. Devonian brittle deformation of caledonized Proterozoic gneiss, Øygarden Complex, SW Norway.

Faulting by activation of preexisting structures

The importance of preexisting planar structures during fault initiation has been pointed out by several authors (Segall and Pollard, 1983; Martel et al., 1988; Bürgmann and Pollard, 1994; Peacock, 2001; Crider and Peacock, 2004; Pollard and Fletcher, 2005). Preexisting structures that can localize strain and guide fault growth are shear zones, joints, veins, bedding and dike walls. Reactivation of earlier faults is not included here, as in this case a fault is already established. Joints are perhaps the most common structure (excluding preexisting faults) that influence fault nucleation. Segall and Pollard's (1983) study from the Sierra Nevada, California, is a benchmark example of the importance of faulting by joint reactivation. Because joints tend to be steep, they are easily activated as strike-slip faults, given that their strike is favorably oriented with respect to the new active stress field. However, steep joints reactivated as subvertical faults or slip surfaces are also very common, generating steep faults or fault elements with complex geometries. Faulted joints are recognized primarily by striated joint surfaces and also give faults or fault segments an unusually planar geometry. They differ from primary faults by

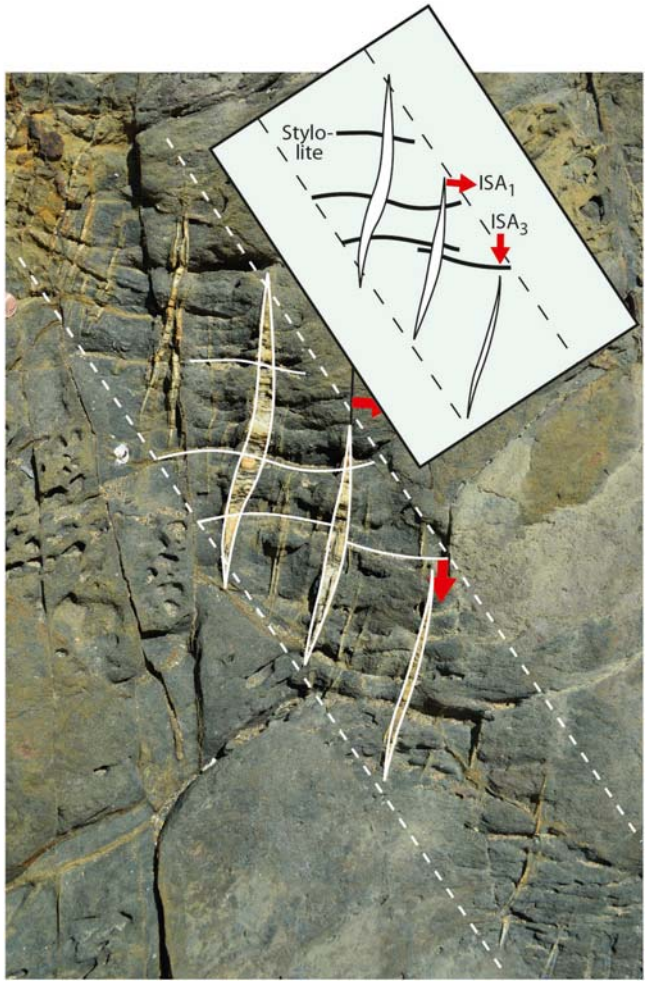

FIGURE 8.16 En-echelon veins accompanied by stylolitic surfaces. ISA – instantaneous stretching axes.

having an initial length that is dictated by the length of the joint. Hence, they are characterized by low displacement/length (D/L) ratios (Wilkins et al., 2001). Faults formed by joint reactivation can result in a single sharp slip surface that lacks subsidiary structures such as Riedel shears, with virtually no fault core or damage zone. As the fault outgrows the joint, however, complications occur, and damage zone and fault core are established and grow. An outstanding example of faulting by joint reactivation is the fault population in the grabens area of Canyonlands National Park, Utah (McGill and Stromquists, 1979). This young fault population formed close to the surface in a ~500 m thick sedimentary sequence containing sandstone layers by faulting of joints belonging to very regularly oriented and spaced joint sets (Moore and Schultz, 1999). Consequently, the faults are very straight, but locally take on zigzag geometries as they exploit different joint sets (Cartwright and Mansfield, 1998). Also, bedding and other lithologic contacts can be reactivated when favorably oriented, as in the example shown in Fig. 8.18.

Many plastic (ductile) shear zones show evidence of brittle reactivation, particularly large shear zones with extensive length and width. The reason why faults preferentially initiate on shear zones is related to the mechanical anisotropy that occurs on a range of scales, from microfabrics through outcrop-scale foliation and mylonitic banding (weak mica-rich layers and stronger quartz-feldspar layers) and contacts between lithologic units with highly different properties, to crustal-scale anisotropy represented by major shear zones (e.g. White et al., 1986). Furthermore, large shear zones represent continuous tabular structures that cut through large portions of the crust. By nucleating on such shear zones, faults can avoid the complicating effect of mechanical stratification and irregularities that generally characterize the crust.

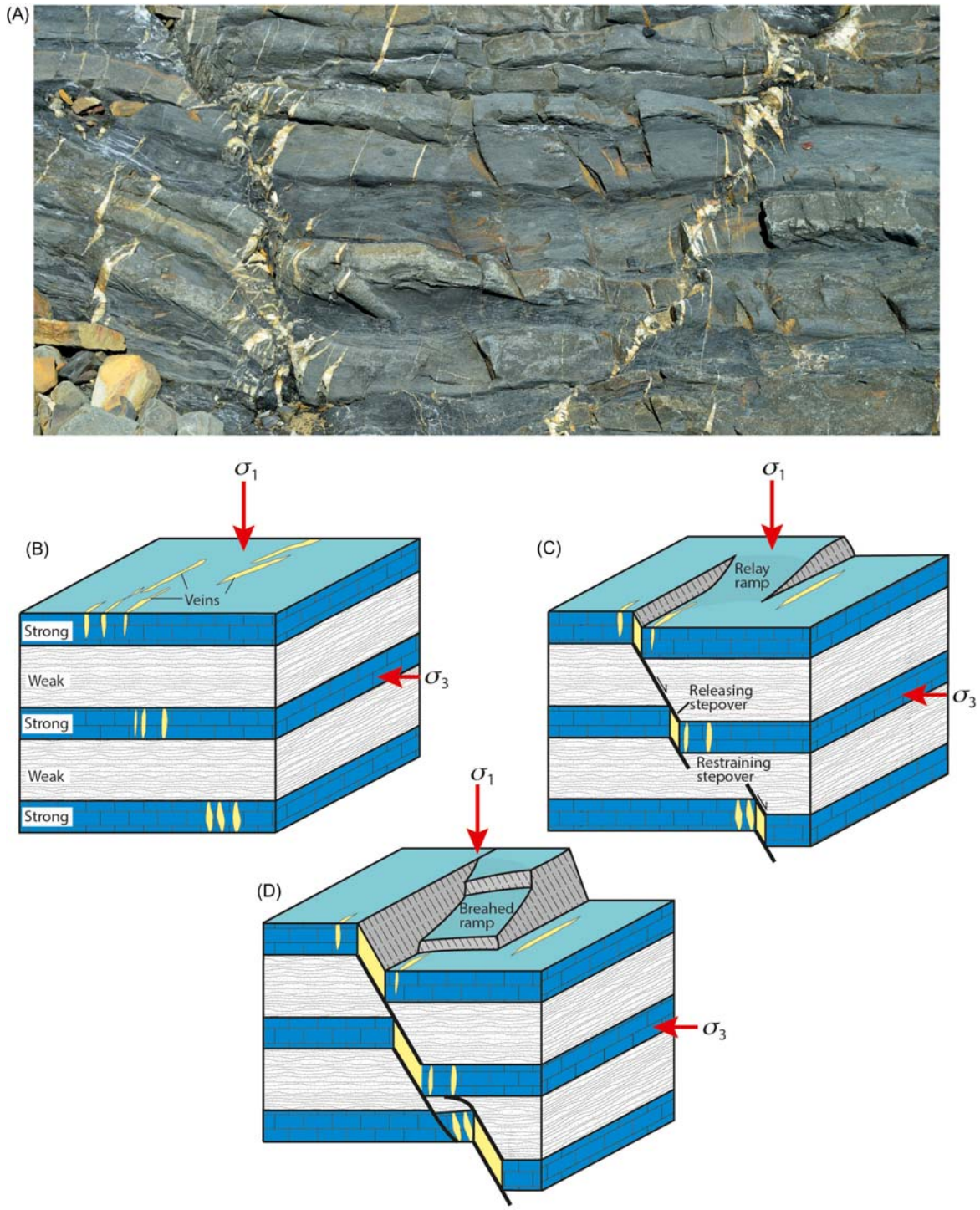

FIGURE 8.17 (A) Two conjugate incipient faults forming by linkage of veins formed preferentially in strong layers. (B–D) Schematic illustration of fault formation from rocks with alternating strong and weak layers: Veins form in strong layers (A) and faults form as shear fractures connect veins in different layers (B and C). Source: *(B–D) Modified from Crider, J.A. Peacock, D.C.P., 2004. Initiation of brittle faults in the upper crust: a review of field observations. J. Struct. Geol., 26, 691–707.*

FIGURE 8.18 Activation of bedding planes as slip surfaces in tilted carboniferous turbidites during Triassic rift-related faulting. The unconformity and Triassic sediments reveal the faulting (Near Sagres, Portugal).

Fault growth

Faults grow by repeated seismic rupture and by more continuous aseismic creep. The San Andreas Fault, for example, has a long section that accumulates slip primarily by creep, flanked by seismically active segments (e.g. Scholz, 2002; Titus et al., 2006). In both cases, displacement accumulates over time, and faults tend to get longer and taller. This is reflected by the positive relationship between displacement and length that can be established for most fault populations (Fig. 8.13). Faults can grow from small fractures that propagate laterally and vertically as they accumulate slip, or they can grow by (re)activation of preexisting structures such as older joints or faults. The first case is an idealized case where (re)activation of preexisting structures is negligible, and where the faults grow in isolation until they incidentally interact. This model has been referred to as the isolated fault model (Walsh et al., 2003). Such growth can be studied in physical or numerical models devoid of preexisting structures.

In nature, preexisting structures are always present and can significantly influence fault growth, as discussed above. For instance, reactivated joints or weak older faults easily accumulate slip along their entire length, creating early-stage faults that are long relative to their maximum displacement. Such underdisplaced faults will accumulate displacement without tip propagation, until they reach a D/L ratio that concentrates enough differential stress at the tip that propagation can occur. Hence, they can be expected to create vertical (constant L, increasing D) paths in diagrams such as Fig. 8.13 until they start to propagate beyond the tipline of the preexisting joint. Data supporting such a joint reactivation model in sandstone are provided by Wilkins et al. (2001).

Low D/L ratios also characterize incipient and small faults in porous rocks, where faults form in or along deformation band clusters. In these cases, the deformation band clusters, which are then precursor structures, follow the trend of cataclastic deformation bands shown in Fig. 8.13, and once a continuous slip surface forms along this zone, it becomes an underdisplaced fault. Again, displacement can be expected to accumulate while the length remains unchanged until a normal D/L ratio is obtained (Fossen and Hesthammer, 1997). From this point onwards, their tips propagate within a tip damage zone of deformation bands that is maintained ahead of the slip surface (Shipton and Cowie, 2003; Fossen et al., 2007) and typically link up with adjacent structures.

It is useful to know how fast displacement varies along a fault when predicting fault displacement or minimum fault length away from an observation point (Fig. 8.11C). The average displacement gradient is around 0.1−0.01 for most normal faults (Fig. 8.19). For a gradient of 0.1 or 0.01, moving 1 km along strike changes the displacement by 100 or 10 m, respectively, provided that we do not cross the D_{max} point. As can be seen even from the simple fault presented in Fig. 8.11B and C, the gradient can change locally along a fault, and the average gradient can only be used as an approximate estimate of displacement variation, for instance away from a well location. It should also be noted that individual data sets tend to show a smaller range in displacement gradient than the global data set (Fig. 8.19). Hence, there are region-specific differences that may relate to mechanical stratigraphy, lithology, degree of linkage, strain (2D vs 3D) and tectonic regime that influence on the displacement gradient of the fault.

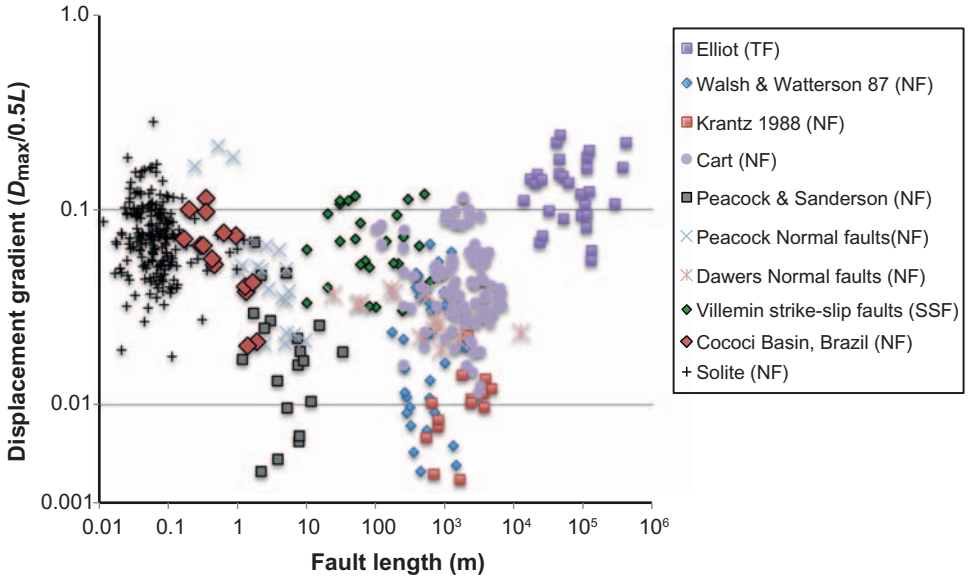

FIGURE 8.19 Average displacement gradient ($D_{max}/(0.5L)$) plotted against fault length for a variety of fault populations in logarithmic diagram. TF – thrust faults and NF – normal faults. Majority of the data show gradients between 0.1–0.01, but each fault population occupy a narrower range than the whole data set.

Fault interaction and linkage

Linkage of faults and fractures occurs at almost any scale, from the linkage of microcracks to form mesoscopic shear fractures (Reches and Lockner, 1994; Crider, 2015) via the linkage of R–R′ structures shown in Fig. 8.14 to the linkage of large fault segments up to hundreds of kilometers long (Peacock et al., 2000). Linkage is a fundamental process of fault growth and can be observed in any tectonic regime and setting, including thrust (Nicol et al., 2002), strike-slip (Woodcock and Fisher, 1986) and various extensional settings. The latter will be the focus of the following discussion.

Whether fault segments form in isolation or by reactivation of older structures, they will at some point interact with other faults and link up to form much longer faults. In the isolated fault model, this is considered a random process, but the position and growth of the linking segments can be controlled by preexisting structures. In either case, the linkage history starts when the fault tips get close enough that their zone of stress perturbation or elastic strain fields overlaps and influences their propagation paths. As the fault tips pass each other, a relay zone develops that is characterized by complex small-scale (subseismic) deformation structures, and layers are bent during the fault interaction. Steepening of the displacement profiles by up to 2.5 times the normal displacement gradient characterizes this stage, indicating a reduction in the tip propagation rate (Peacock and Sanderson, 1996; Gupta and Scholz, 2000). This goes together with the observation that the displacement profile of each fault becomes skewed, with maxima shifted towards the relay structure (Fig. 8.12D). The geometry of relay structures are scale-independent, with a common length:width ratio of around 3–4 (Long and Imber, 2011) (Fig. 8.20). Fault growth by linkage is easily documented by simple physical experiments, such as the plaster experiment shown in Fig. 8.21. Here, several small segments (F2a–d in Fig. 8.21A) link up to form a longer fault (F2 in Fig. 8.21B), which after its formation accumulates displacement without lengthening (from Fig. 8.21B and C). Extension beyond the stage shown in Fig. 8.21C would break the ramps between segments F1–F3 and repeat the history of F2 at a larger scale to form a continuous curvilinear F1–F3 fault trace.

A relay structure or relay zone represents an anomalously wide portion of the fault damage zone sheared by the two overlapping fault segments. The types of subsidiary structures developed in a relay zone depends largely on lithology and may encompass deformation bands, slip surfaces, extension fractures, stylolites, veins, dikes and minor faults, as described in several recent publications (e.g. Trudgill and Cartwright, 1994; Peacock and Sanderson, 1995; Acocella et al., 2000; Rotevatn et al., 2007; Bastesen and Rotevatn, 2012; Fossen and Rotevatn, 2016). Their density and connectivity depend on the maturity of the relay zone, that is the amount of strain or displacement accommodated in the zone. Eventually, the two overlapping faults will breach the relay ramp to

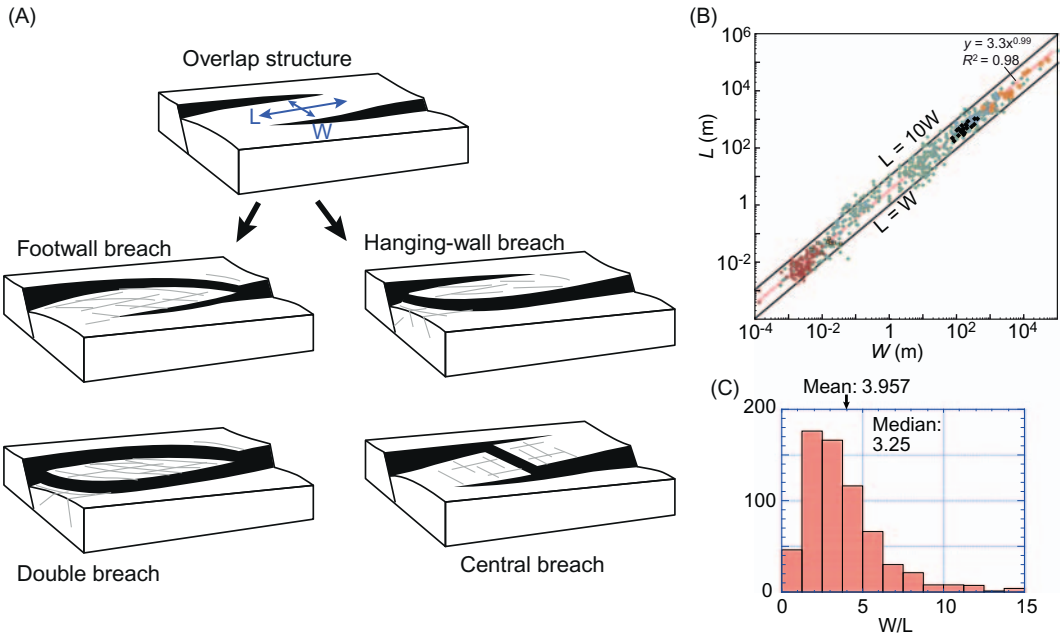

FIGURE 8.20 (A) Fault overlap structure (relay structure) created by two subparallel fault tips. The structure may be breached in different ways; four general scenarios are shown. (B) relay length scales with width over at least nine orders of magnitude, that is ramps are a self-similar type of structure. See Fossen and Rotevatn (2016) for data sources. (C) Statistical distribution for data plotted in (B), describing the range in L/W ratio reflected by the scatter in (B).

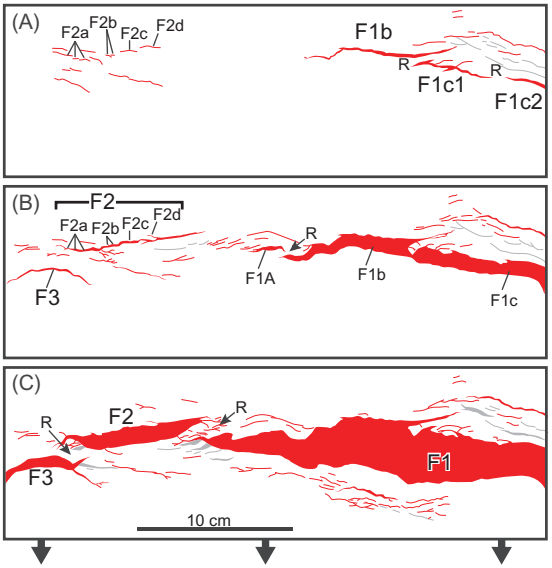

FIGURE 8.21 Progressive evolution of fault zone produced in extensional plaster model (black arrows indicate the extension direction). Multiple small faults in (A) propagate and coalesce by linkage as strain accumulates. (B) Intermediate stage where several faults have coalesced to form three larger faults (F1–F3). Note that linkage points are preserved as pronounced jogs in fault trace. (C) At this stage, the tip of F1 has propagated by linkage of smaller faults, while F2 and F3 have experienced constant length (*L*) growth. If the experiment had continued, F1–F3 would have linked up to a single continuous fault. Several breached relays can be recognized by fault jogs. Source: *Redrawn and modified from Blækkan, I., 2016. Evolution of normal faults and fault-related damage: insights from physical experiments, Master thesis, University of Bergen. p. 86.*

form a continuous fault structure. Single-tip or double-tip breaching is possible, and further slip accumulation on the composite fault will leave much of the relay ramp inactive. The new and much longer fault will initially be underdisplaced, and a displacement minimum may exist for some time at the linkage point (Faure Walker et al., 2009). In the length-displacement diagram (Fig. 8.13), linkage results in rapid increase in length of the new combined fault followed by an increase in maximum displacement while the length remains unchanged, that is a horizontal, then vertical path (Fig. 8.12D) (Cartwright et al., 1995). Hence, growth by linkage can explain some of the scatter in length-displacement diagrams. For lateral linkage controlled by upward propagation of underlying structures, however, the minima may be erased at initial stages of linkage, and such fault systems are referred to as kinematically coherent (Walsh et al., 2003).

In general, fault growth by linkage is considered the most efficient and common way for faults to grow in length. It also occurs in the vertical (dip) direction, as already indicated in Fig. 8.17, as well as in any other direction. In a more or less horizontally layered sequence, layering plays an important role. Mechanically contrasting layers may cause faults to initiate at different stratigraphic levels during strain accumulation, and extensive linkage occurs as they connect and grow into larger faults. Fig. 8.17 shows how this can influence the width of the fault zone. Field observations (Fig. 8.22) show a large variation in both fault core and fault damage zone width in the vertical direction that can be explained by vertical coalescence of fault segments. Hence, the resulting fault complications and variations in damage zone width and properties depend on lithology, the mechanical properties of the layers, their thickness, progressive fault rotation and fault displacement (e.g. van der Zee et al., 2008). Further work is needed on the role of these factors to obtain a useful algorithm for fault damage zone prediction.

Indeed, faults with any orientation can interact, and they can do so in different ways (Fossen et al., 2005). Conjugate systems and subparallel faults are already covered above, but abutting situations where one fault terminates against another are also very common. In this case, a fault tip approaches an already existing fault and terminates against it. When both faults are active, the new fault will link up to form a kinematically coherent system of three blocks and a Y-type fault intersection. An example is shown in Fig. 8.23, where also another common feature is seen, known as fault tip deflection near an existing weak fault. This rotation reflects the stress rotation that occurs around weak structures (e.g. Dyer, 1988), and the fault propagating into the perturbated local stress field of an existing fault may result in a curved fault, as shown in Fig. 8.23B and C. Field examples show that these types of locations can display quite complicated patterns of small-scale structures with a multitude of orientations and even types of structures, in an anomalously wide damage zone. In the area covered by Fig. 8.23, comparison between single fault damage (e.g. location BC) and areas of fault interaction (location CR in Fig. 8.23) demonstrates this fact well, as illustrated somewhat schematically in Fig. 8.24 (see also Johansen et al., 2005).

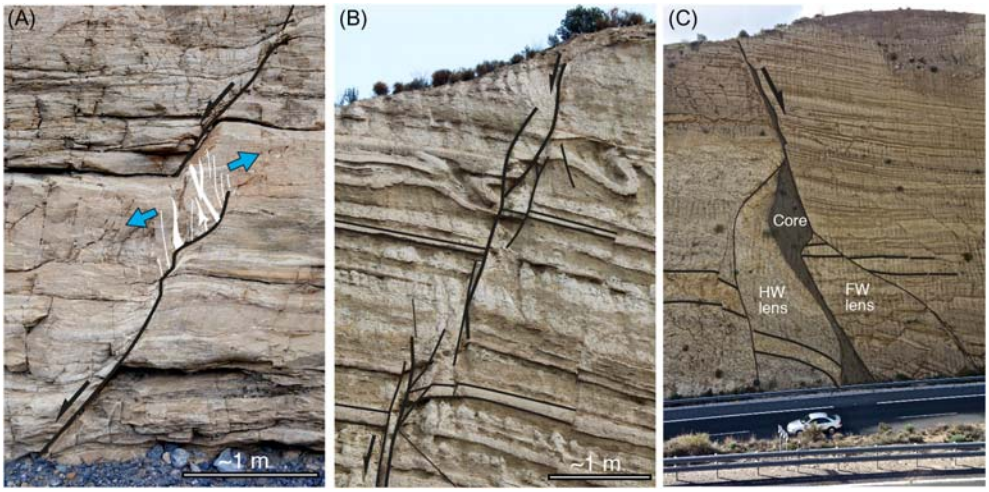

FIGURE 8.22 Three faults at different stages of evolution, each consisting of several subsidiary elements. (A) Two faults linking up vertically, forming a releasing (extensional) stepover. Extension indicated by veins. Marble Canyon, Death Valley. (B) Fault zone established along minor (meter-scale) fault, cutting soft-sediment folds. Vertical linkage not completed yet. (C) Mature fault with approximately 100 m offset, with well-developed fault core and lenses. Latter two examples are from the Neogene-Quaternary Granada Basin, Spain.

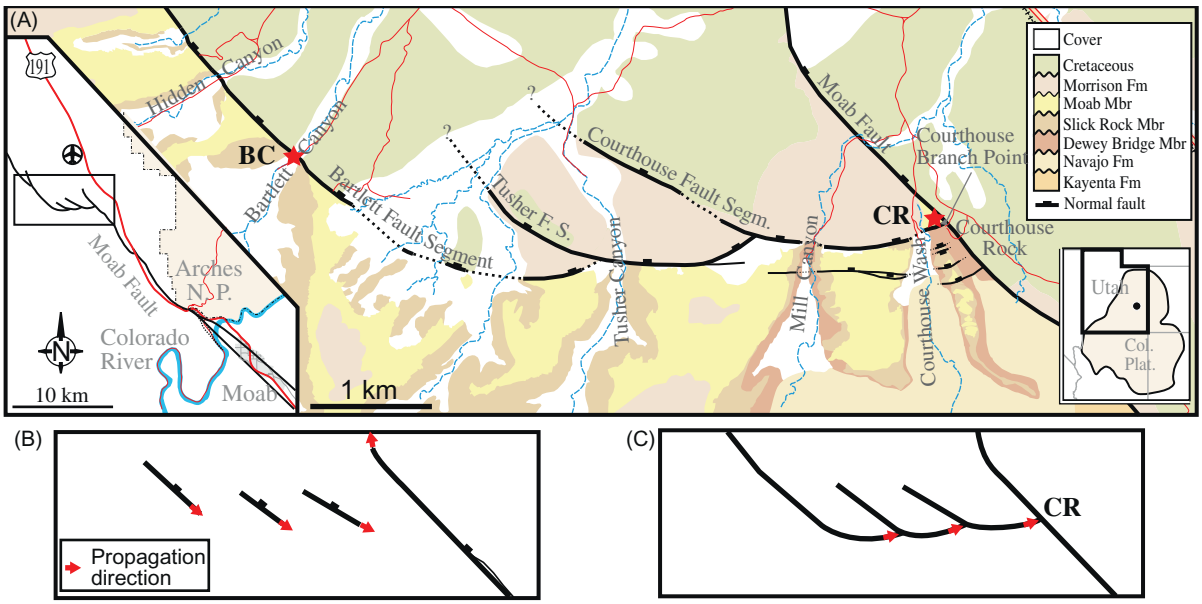

FIGURE 8.23 The northernmost part of the Moab Fault and a series of connecting subsidiary fault segments (A). The evolution of these segments is interpreted in B–C, and involves tip deflection related to stress perturbation near neighboring faults. Hence, the curvature of the southeastern Courthouse fault segment formed because of the already established Moab Fault. Also, the displacement of the Courthouse fault segment decreases towards the linkage point with the Moab Fault (CR), consistent with an abutting history. CR – Courthouse Rock locality and BC – Bartlett Canyon locality.

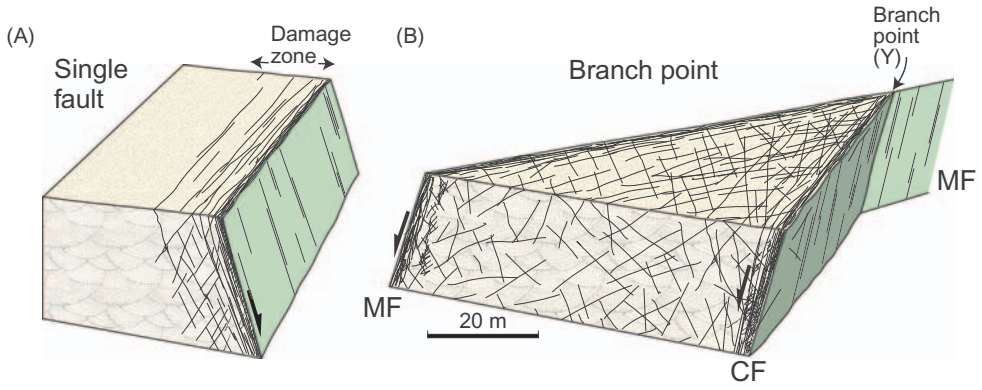

FIGURE 8.24 (A) Single fault damage and (B) the more complicated Y-point (abutting) branch point situation. These two situations correspond to the BC and CR locations in the previous figure. The BC damage zone is illustrated in more detail in Fig. 9.13 in Fossen (2016), while the CR branch point situation is presented in detail by Johansen et al. (2005).

Fault populations

Faults form populations that develop from a multitude of small faults to a more diverse population consisting of faults with a large range of displacements and lengths. As already emphasized, this evolution involves linkage of small faults to larger ones, where the largest faults take up most of the subsequent strain (e.g. Cowie, 1998) (Fig. 8.25). The early small faults that are not involved in such linkage will then become inactive. The extent of

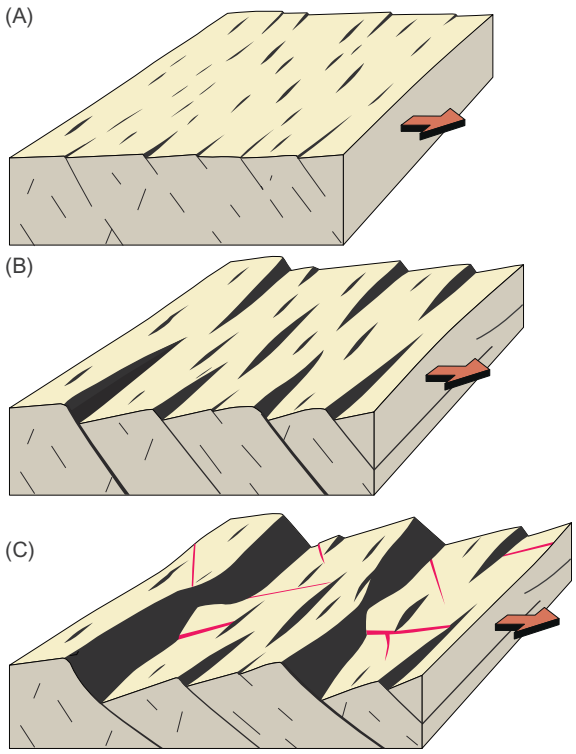

FIGURE 8.25 Schematic illustration of the evolution of a fault population in an extensional (rift) setting. (A) Initial population of minor isolated faults developing largely perpendicular to the extension direction. (B) Some growth by fault tip propagation creates zones of fault overlap. (C) Linkage of favorably arranged segments into long- and large-offset faults, with secondary formation of adjustment faults (red) between the large faults. Note that the late minor faults typically show a large variety of orientations, commonly trending at a high angle to the large faults.

linkage varies within the deformed region, and after some strain has been accumulated, there will be a distribution of fault sizes that in many cases can be described by a power-law relationship of the form $N = aS^{-D}$, where S represents a fault size parameter such as displacement or length, N is the cumulative number of faults greater than or equal to S, a is a constant and D is the power-law coefficient or fractal dimension that characterizes the relative proportion of large and small faults in the population. D can be used to assess the amount of strain represented by different size ranges of a fault population, including subseismic faults. The amount of subseismic deformation depends on seismic resolution and can be substantial where regional data are considered (see Marrett and Allmendinger, 1992 and Walsh and Watterson, 1992 for further discussion).

In terms of distribution, the largest faults in a faulted region commonly develop a regular pattern with a characteristic spacing. This spacing is in part controlled by the mechanical thickness of the relevant layer, which for very small faults could be the thickness of a competent sandstone or limestone layer. For larger faults, the relevant layer may comprise a supra-salt sequence, supradetachment hanging wall or thrust nappe, while for first-order faults with several kilometers of displacement, the relevant layer may comprise the entire brittle crust. Soliva et al. (2006), who considered this relationship primarily for small faults, found that spacing is typically about half of the relevant layer thickness. For a 10 km thick brittle crust, this fits well with the ~5 km average spacing observed in most rifts (Morellato et al., 2003).

Even though a multitude of small faults form at early stages of rifting, most of which become inactive, small faults also form at later stages. Once larger faults are established, small faults and related deformation structures will potentially form in the fault blocks between these faults in response to complications during further deformation. In terms of stress, this can be explained by the way the existing faults perturb the regional stress field due to their geometry and relative movements. Hence, both the locations and orientations of new faults will be controlled by the existing faults and their geometries. Maerten et al. (2002) and Maerten and Maerten (2006) used geomechanical modeling to make predictions about such smaller-scale faults. They applied a 3D numerical model to determine the stress conditions in an area containing active N–S trending North Sea rift faults. The computed stress field around and between the larger faults was then combined with a Coulomb failure criterion to predict

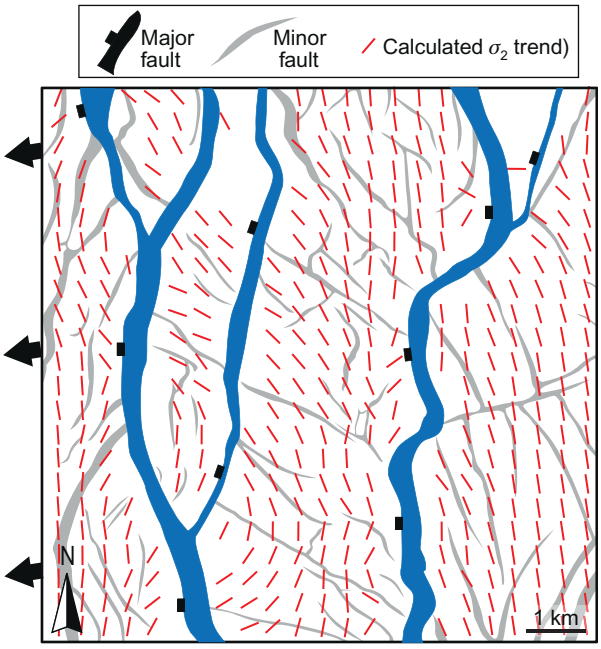

FIGURE 8.26 Numerically modelled stress field during E–W extension in the Oseberg Syd area, northern North Sea. The blue faults perturb the stress field, and many of the minor (red) faults are oriented in agreement with the local orientation of σ_2. Hence, many minor faults and their great variety of orientations can be explained as having formed after the blue faults were established (but during the same phase of rifting). Source: *Modified from Maerten, L., Gillespie, P. Pollard, D.D., 2002. Effects of local stress perturbation on secondary fault development. J. Struct. Geol. 24, 145–153.*

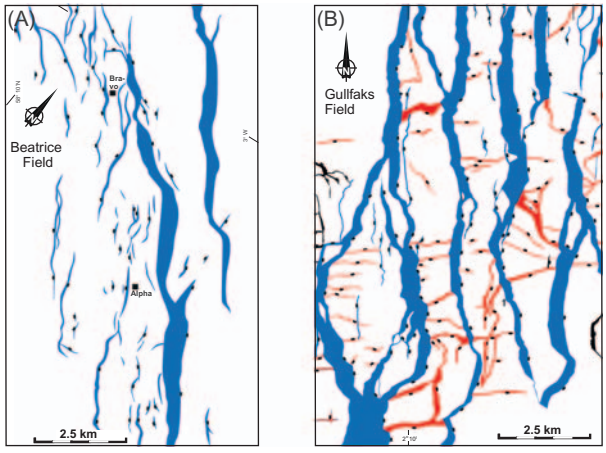

FIGURE 8.27 Two fault patterns from the North Sea rift, at two different stages of development. (A) The Beatrice Field (Inner Moray Firth Basin) where the majority of faults are subparallel and perpendicular to the extension direction. (B) The Gullfaks Field, where several small faults bound by the larger N–S trending faults have different orientations, making Y- and T-branch points with the N–S faults. Many of the red-colored faults may have formed at a relatively late stage of extension, due to kinematic complications caused by slip on the larger faults. Source: *(A) Fault pattern extracted from Husmo, T., Hamar, G.P., Høiland, O., Johannesen, E.P., Rømuld, A., Spencer, A.M. et al., 2002. Lower and Middle Jurassic. In: Evans, D., Graham, C., Armour, A. & Bathurst, P. (Eds.), The Millennium Atlas: Petroleum Geology of the Central and Northern North Sea. Geological Society, London, pp. 129–155. (B) Fault pattern from Fossen, H., Rørnes, A. 1996. Properties of fault populations in the Gullfaks Field, northern North Sea. J. Struct. Geol. 18, 179–190.*

the orientations and densities of smaller faults. The result (Fig. 8.26) shows a population of smaller faults with a large range in orientation, in part similar to the small-scale faults identified from seismic interpretation, and quite different from the N–S trending major faults.

A somewhat similar fault pattern is observed in the Gullfaks Field fault population in the North Sea rift (Fig. 8.27B), where N–S trending domino-style rift faults separate smaller faults with many different orientations, many oblique or perpendicular to the larger faults (red faults in Fig. 8.27B). These small faults abut the larger faults

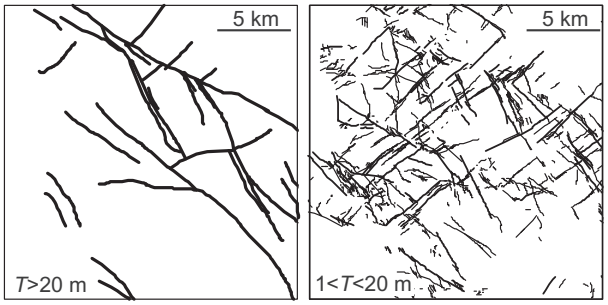

FIGURE 8.28 Fault pattern mapped from a 20 by 20 km^2 area from the East Pennine Coalfield, United Kingdom. The orientation defined by faults with throw (T)>20 m are not repeated by smaller faults. Instead, smaller faults show a large subpopulation of NE–SW trending faults. This comparison shows the challenges of predicting small-scale faults from fault pattern defined by larger faults. Source: *Modified from Bailey, W.R., Walsh, J.J. Manzocchi, T., 2005. Fault populations, strain distribution and basement fault reactivation in the East Pennines Coalfield, UK. J. Struct. Geol., 27, 913–928.*

and clearly formed in the same tectonic phase, but after the large faults were already established. Kinematically, these minor faults appear to be adjustment or release structures formed within the relatively long and narrow domino fault blocks as they deform internally due to geometric irregularities and differential slip on the larger domino-style rift faults. Hence, a simple first-order model for the fault development in such fault arrays is an early stage of extension-perpendicular faults (Fig. 8.25A), establishment of some long faults by linkage (Fig. 8.25B), and then the formation of new small faults in the fault blocks between these large faults (Fig. 8.25C). This model is related to strain, and the case of Fig. 8.27A, which shows mostly N–S faults, will probably develop into a fault pattern more similar to the Gullfaks (Fig. 8.27B) or Oseberg Syd (Fig. 8.26) examples.

An important consequence of this evolution is that not all properties of large faults can be assumed to be valid also for smaller faults in the same region. In particular, small faults may have completely different orientations and distributions. Hence, small faults cannot uncritically be predicted from knowledge of regional stress or strain fields or by downscaling of larger fault patterns, even if they formed in the same regional strain field. Bailey et al. (2002) showed an example that can be related to seismic resolution, which typically is around 10–20 m for many reflection seismic surveys (i.e. faults with displacement <10–20 m not being detectable). The map showing only faults with maximum throw <20 m is remarkably different from the pattern defined by larger faults (Fig. 8.28), and small faults are thus very difficult to predict from the large fault pattern. For cases where the principal stretching directions change orientation during deformation, for example extension direction changing during a rift phase, further complications are expected to arise.

In summary, fault populations or networks that show several different fault orientations can form in many ways: (1) by local stress variations during deformation, as illustrated in Fig. 8.26; (2) by a change in the regional stretching directions during deformation; (3) by two or more deformation phases with differently oriented stretching directions; or (4) by reactivation of preexisting structures. Distinguishing between these cases largely relies on crosscutting relations and tectonostratigraphic constraints. Crosscutting relations can in some cases be difficult to map from seismic data and require high-quality data and detailed structural analysis (e.g. Duffy et al., 2015). Tectonostratigraphic constraints, for instance where a set or subset of faults is absent in the younger part of a sequence or if strain changes abruptly across a given stratigraphic level, are usually easier to identify and employ. If the deformation history is not clear, the first approach should be to try to explain all elements of a fault population with a single phase of deformation (Fossen et al., 2019), for instance with the aid of a geomechanical modeling tool (Maerten et al., 2002), balancing techniques/kinematic analysis, topological considerations (Duffy et al., 2017) and modeling of different scenarios of reactivation (Henza et al., 2010; Deng et al., 2017, 2018).

Faults and fluids

Faults and fractures have two important properties; they represent mechanical discontinuities and they generally conduct fluids. While the first is important to fault reactivation potential, it also relates to their ability to conduct water, oil, gas and magma. Flow of fluids along faults and fault networks generate ore deposits, water resources in solid rock, hydrocarbon deposits, cause leakage of hydrocarbon traps, and guide magma and can control the locations of volcanoes and hydrothermal springs. The field is wide and complex, and only a few fundamental considerations are presented here.

Faults behave differently in porous and nonporous (e.g. magmatic and metamorphic) rocks. In porous rocks, faults have very different properties in different directions. Cross-fault flow is commonly retarded or stopped by the fault gauge of the fault core or by unfavorable stratigraphic juxtaposition (e.g. sandstone against shale; Færseth, 2006). At the same time, the fault can conduct fluids in the vertical direction.

Faults that prohibit cross-fault fluid flow are sealing, and their sealing capacity depends on several factors. First, the amount of offset is important because more offset generally produces more and thicker fault rock (fault core) (Fig. 8.5). On the contrary, where shale smear is the seal-forming mechanism, increasing offset also increases the probability of smear discontinuities that represent leakage points across the fault. Second, the presence of shale is important because of the likelihood of shale smear formation. The shale smear potential is commonly evaluated from simple equations that involve the ratio between the thickness of the shale layer(s) involved and the fault offset. This is a simple first-order approach and should be used together with case-specific variables such as burial depth, cementation, shale type, other fault rocks involved, burial/uplift history and so on (Knipe et al., 1997). Third, juxtaposition, which is a function of fault offset, fault zone architecture and stratigraphy, is important primarily because a fault or portion of a fault where reservoir is juxtaposed against itself (self-juxtaposition) is much less likely to be sealing than any other case. In the case of self-juxtaposition, only a fault rock can provide a seal, which is unlikely unless intense cataclasis is involved. Where reservoir is juxtaposed against stratigraphically higher or lower reservoirs, sealing is controlled by smearing of nonreservoir units. Smear is most effective if those units are represented by shale or clay. Fault seal-controlling factors vary along faults, and fault surface maps showing variations in juxtaposition, fault rock properties and shale smear factor can be made to analyse the sealing potential of a fault in three dimensions (Cerveny et al., 2004). For more information about fault sealing, see Fisher and Knipe (2001), Færseth et al. (2007) and Sperrevik et al. (2002).

In the vertical direction, through-going slip surfaces and, less commonly, permeable gouge provide continuous fractures that can open under elevated fluid pressures. Thus faults provide an important means for fluids to move vertically through the brittle crust. Preferred cementation and mineralization along faults, such as the red-colored fault zone seen in Fig. 8.29, are evidence of this. Faults as vertical pathways for fluids can be positive in the context of vertical migration from the source rock into stratigraphically higher reservoir rocks. It can also contribute to vertical communication in an alternating sand-shale type reservoir (e.g. Bailey et al., 2002). However, in the context of hydrocarbon traps, faults that cut the top seal (caprock) can cause hydrocarbons to migrate out of the structure and hence deplete or empty the trap.

The influence of faults on fluid flow in a sedimentary basin is closely related to their geometry, connectivity, distribution and orientation (Fig. 8.30) and hence to their evolution. Laterally segmented fault systems may contain unbreached relay ramps that provide fluid communication across fault blocks. Vertical segmentation with associated smear reduces both vertical and horizontal communication. On the other hand, fault zones that

FIGURE 8.29 Steep fault cutting sedimentary layers along the flank of the Bighorn Mountains, Wyoming, exposing red color due to iron oxidation by fluids flowing along the fault.

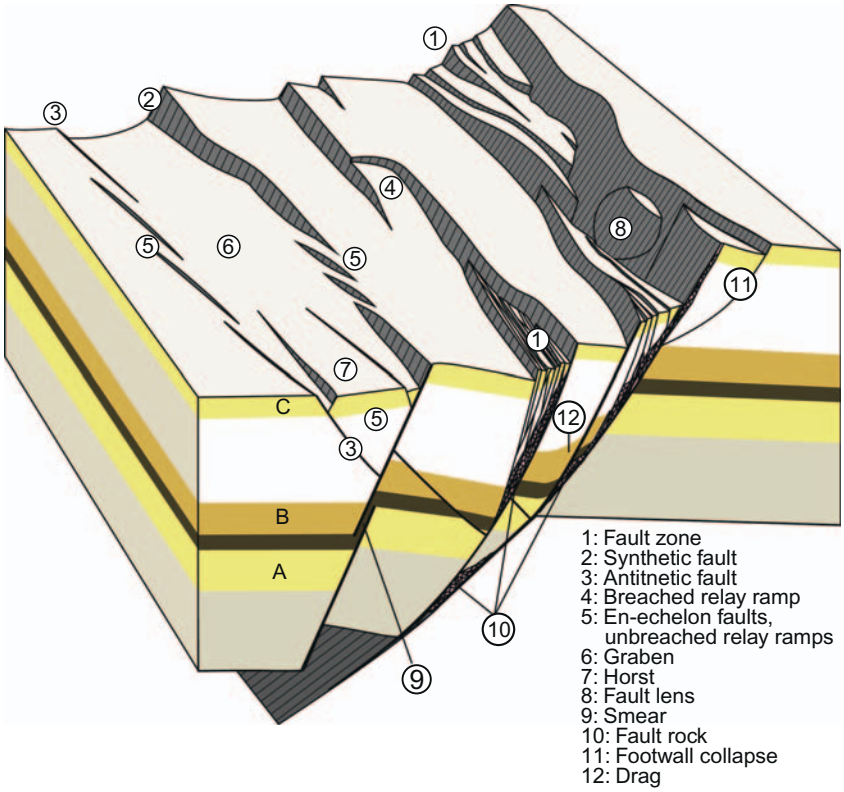

FIGURE 8.30 Some typical structural complexities associated with normal faulting, as discussed in the text. Source: *Inspired by Wibberley, C.A.J., Shipton, Z.K. 2010. Fault zones: a complex issue. J. Struct. Geol. 32, 1554–1556.*

distribute offset over several fault elements generally (but not necessarily) improve communication across faults. Variations in these features along strike, related to the history of lateral linkage during strain accumulation, are also important, and any consideration of communication must be 3D to be realistic. Fig. 8.30 summarizes typical structures that are relevant for communication in faulted reservoirs.

Faults in nonporous rocks are conduits of fluids, and the damage zone is usually more important than the tight core, as it consists of well-connected fractures that can conduct fluids. Near the surface, such zones are exploited for water. Deeper down, they transport hotter fluids that can deposit minerals and elements of economic interest. Fluid flow depends on fracture density and connectivity, both of which tend to be higher in fault relays, branch points (Fig. 8.24) and transfer zones. Hence cementation, hot springs, hydrothermal activity and volcanic activity are concentrated in such locations at a range of scales (Bastesen and Rotevatn, 2012; Corti, 2012). For instance, concentration of geothermal fields in fault stepovers has been reported by Rowland and Sibson (2004) in a segmented rift system in New Zealand. Increased geothermal fluid activity in fault linkage zones was also reported by Curewitz and Karson (1997) and by Dockrill and Shipton (2010) who showed that CO_2 springs and seeps were colocated with structurally complex zones in a fault array. Further, magma emplacement has been correlated with dilational jogs or transverse fault relays (Vigneresse and Bouchez, 1997) and extensional transfer zones (Dini et al., 2008; Corti, 2012). As for economic geology, the copper mineralization along the Lisbon Valley Fault and the Dolores fault zones in Utah and Colorado (Breit and Meunier, 1990) are localized at relay zones, and hydrocarbon leaks are preferentially found along fault relays and intersection points (e.g. Gartrell et al., 2004). Furthermore, fault jogs, which commonly represent the locations of previous fault linkage zones, correlate with hydrothermal gold deposits in strike-slip systems (Micklethwaite and Cox, 2004, 2006).

Finally, it is to be emphasized that deposition of minerals from fluids circulating in fault networks generally leads to a decrease in fault and fracture permeability. Predicting the extent and thereby the influence of mineralization or cementation on permeability is difficult. In many cases, mineralization develops faults into baffles rather than sealing structures. In addition, fault reactivation will generally break the seal and enhance permeability. Thus, in exploration and reservoir evaluations, it is important to relate fault orientation to the in situ stress field in order to predict their reactivation potential.

Concluding remarks

Faults are important structures in the upper part of the crust and show wide ranges in size, geometry, anatomy and properties. They develop from small-scale secondary structures that form in a brittle shear zone at an angle to the shear zone boundaries (trend of future fault zone) and that link up to form larger faults that typically develop a core or slip surface surrounded by a volume of deformed rock (damage zone). However, they also form by (re)activation of preexisting structures such as joints, dikes, lithologic contacts and foliations where such structures introduce significant rock anisotropy. Growth by linkage is extremely common and important during fault growth and cause rapid lengthening of faults and formation of large faults that control much of the subsequent strain accumulation. It also creates variable damage along faults, with wider and composite damage around linkage sites. Furthermore, geometric complications at these sites can create anomalous stress patterns during continued slip accumulation that produce new faults with orientations that deviate from that of the larger faults.

Linkage processes and relay structures also strongly control the sealing properties of faults; vertical segmentation creates shale smear, while lateral ramp formation tends to create pathways for fluids across faults and also vertically in rocks with little or no primary porosity. Hence, understanding fault linkage processes is important for hydrogeological as well as economical and hydrocarbon exploration purposes. In general, a fault population form unconnected or connected elements that change characteristics as more strain accumulates. In general (with some exceptions), connectivity is enhanced, compartmentalization of porous reservoirs increases, communication in nonporous reservoirs increases and the pattern of reservoir juxtaposition changes. In conclusion, faults and their properties are largely dictated by their initiation and early history together with lithologic properties, including preexisting structure. For instance, distribution of incipient faults influences future linkage patterns and fault geometries, which again influence stress perturbations that create new faults. Hence, studies of fault initiation and evolution through time form an important field of research and should continue to receive attention through numerical modeling, experimental work, field mapping and interpretation of seismic data.

Acknowledgments

CGG are thanked for permission to publish seismic examples in Fig. 8.7. Constructive review by Jürgen Adam is highly appreciated.

References

Ackermann, R.V., Schlische, R.W., Withjack, M.O., 2001. The geometric and statistical evolution of normal fault systems: an experimental study of the effects of mechanical layer thickness on scaling laws. J. Struct. Geol. 23, 1803–1819.

Acocella, V., Gudmundsson, A., Funiciello, R., 2000. Interaction and linkage of extension fractures and normal faults: examples from the rift zone of Iceland. J. Struct. Geol. 22, 1233–1246.

Amilibia, A., Sabat, F., McClay, K.R., Munoz, J.A., Roca, E., Chong, G., 2008. The role of inherited tectono-sedimentary architecture in the development of the central Andean mountain belt: insights from the Cordillera de Domeyko. J. Struct. Geol. 30, 1520–1539.

Anderson, E.M., 1951. The Dynamics of Faulting. Oliver & Boyd, Edinburgh.

Angelier, J., 1979. Determination of the mean principal directions of stresses for a given fault population. Tectonophysics 56, T17–T26.

Angelier, J., 1994. Fault slip analysis and palaeostress reconstruction. In: Hancock, P.L. (Ed.), Continental Deformation. Pergamon Press, Oxford, pp. 53–100.

Bailey, W.R., Manzocchi, T., Walsh, J.J., Keogh, K., Hodgetts, D., Rippon, J., et al., 2002. The effect of faults on the 3D connectivity of reservoir bodies: a case study from the East Pennine Coalfield, U.K. Pet. Geosci. 8, 263–277.

Bailey, W.R., Walsh, J.J., Manzocchi, T., 2005. Fault populations, strain distribution and basement fault reactivation in the East Pennines Coalfield, UK. J. Struct. Geol. 27, 913–928.

Bastesen, E., Rotevatn, A., 2012. Evolution and structural style of relay zones in layered limestone-shale sequences: insights from the Hammam Faraun Fault Block, Suez rift, Egypt. J. Geol. Soc. 169, 477–488.

Berg, S.S., Skar, T., 2005. Controls on damage zone asymmetry of a normal fault zone: outcrop analyses of a segment of the Moab fault, SE Utah. J. Struct. Geol. 27, 1803–1822.

Bird, P.C., Cartwright, J.A., Davies, T.L., 2015. Basement reactivation in the development of rift basins: an example of reactivated Caledonide structures in the West Orkney Basin. J. Geol. Soc. 172, 77–85.

Blækkan, I., 2016. Evolution of Normal Faults and Fault-Related Damage: Insights From Physical Experiments (Master thesis). University of Bergen. 86 pp.

Braathen, A., Tveranger, J., Fossen, H., Skar, T., Cardozo, N., Semshaug, S.E., et al., 2009. Fault facies and its application to sandstone reservoirs. Am. Assoc. Pet. Geol. Bull. 93, 891–917.

Breit, G.N., Meunier, J., 1990. Fluid inclusion, d18O, and 87Sr/86Sr evidence for the origin of fault-controlled copper mineralization, Lisbon Valley, Utah, and Slick Rock District, Colorado. Econ. Geol. 85, 884–891.

Bürgmann, R., Pollard, D.D., 1994. Strain accommodation about strike-slip fault discontinuities in granitic rock under brittle-to-ductile conditions. J. Struct. Geol. 16, 1655–1674.
Caine, J.S., Evans, J.P., Forster, C.B., 1996. Fault zone architecture and permeability structure. Geology 24, 1025–1028.
Cartwright, J.A., Mansfield, C.S., 1998. Lateral displacement variation and lateral tip geometry of normal faults in Canyonlands National Park, Utah. J. Struct. Geol. 20, 3–19.
Cartwright, J.A., Trudgill, B.D., Mansfield, C., 1995. Fault growth by segment linkage: an explanation for scatter in maximum displacement and trace length data from the Canyonlands Grabens of SE Utah. J. Struct. Geol. 17, 1319–1326.
Cerveny, K., Davies, R., Dudley, G., Kaufman, P., Knipe, R.J., Krantz, B., 2004. Reducing uncertainty with fault-seal analysis. Oilfield Rev. 16, 38–51.
Childs, C., Nicol, A., Walsh, J.J., Watterson, J., 1996. Growth of vertically segmented normal faults. J. Struct. Geol. 18, 1389–1397.
Childs, C., Nicol, A., Walsh, J.J., Watterson, J., 2003. The growth and propagation of synsedimentary faults. J. Struct. Geol. 25, 633–648.
Childs, C., Manzocchi, T., Walsh, J.J., Bonson, C.G., Nicol, A., Schöpfer, M.P.J., 2009. A geometric model of fault zone and fault rock thickness variations. J. Struct. Geol. 31, 117–127.
Cloos, H., 1928. Experimente zur Inneren Tektonik. Centr. Mineral. Geol. Paläontol. Abt. B Geol. Paläontol. 609–621.
Corti, G., 2012. Evolution and characteristics of continental rifting: analog modeling-inspired view and comparison with examples from the East African Rift System. Tectonophysics 522–523, 1–33.
Cowie, P.A., 1998. A healing-reloading feedback control on the growth rate of seismogenic faults. J. Struct. Geol. 20, 1075–1087.
Cowie, P., Gupta, S., Dawers, N.H., 2000. Implications of fault array evolution for synrift depocentre development: insights from a numerical fault growth model. Basin Res. 12, 241–261.
Crider, J.G., 2015. The initiation of brittle faults in crystalline rock. J. Struct. Geol. 77, 159–174.
Crider, J.A., Peacock, D.C.P., 2004. Initiation of brittle faults in the upper crust: a review of field observations. J. Struct. Geol. 26, 691–707.
Curewitz, D., Karson, J.A., 1997. Structural settings of hydrothermal outflow: fracture permeability maintained by fault propagation and interaction. J. Volcan. Geotherm. Res. 79, 149–168.
Deng, C., Gawthorpe, R.L., Finch, E., Fossen, H., 2017. Influence of a pre-existing basement weakness on normal fault growth during oblique extension: insights from discrete element modeling. J. Struct. Geol. 105, 44–61.
Deng, C., Gawthorpe, R.L., Fossen, H., Finch, E., 2018. How does the orientation of a pre-existing basement weakness influence fault development during renewed rifting? Insights from three-dimensional discrete element modeling. Tectonics 37, 2221–2242.
Dini, A., Westerman, D.S., Innocenti, F., Rocchi, S., 2008. Magma emplacement in a transfer zone: the Miocene mafic Orano dyke swarm of Elba Island, Tuscany, Italy. Geol. Soc. London Spec. Publ. 302 (1), 131–148.
Dockrill, B., Shipton, Z.K., 2010. Structural controls on leakage from a natural CO_2 geologic storage site: Central Utah, U.S.A. J. Struct. Geol. 32.
Duffy, O.B., Bell, R.E., Jackson, C.A.L., Gawthorpe, R.L., Whipp, P.S., 2015. Fault growth and interactions in a multiphase rift fault network: Horda Platform, Norwegian North Sea. J. Struct. Geol. 80, 99–119.
Duffy, O.B., Nixon, C.W., Bell, R.E., Jackson, C.A.L., Gawthorpe, R.L., Sanderson, D.J., et al., 2017. The topology of evolving rift fault networks: single-phase vs multi-phase rifts. J. Struct. Geol. 96, 192–202.
Dyer, R., 1988. Using joint interactions to estimate paleostress ratios. J. Struct. Geol. 10, 685–699.
Erslev, E.A., 1991. Trishear fault-propagation folding. Geology 19, 617–620.
Etchecopar, A., Vasseur, G., Daignieres, M., 1981. An inverse problem in microtectonics for the determination of stress tensors from fault striation analysis. J. Struct. Geol. 3, 51–65.
Faulkner, D.R., Mitchell, T.M., Jensen, E., Cembrano, J., 2011. Scaling of fault damage zones with displacement and the implications for fault growth processes. J. Geophys. Res. 116 (B5).
Faure Walker, J.P., Roberts, G.P., Cowie, P.A., Papanikolaou, I.D., Sammonds, P.R., Michetti, A.M., et al., 2009. Horizontal strain-rates and throw-rates across breached relay zones, central Italy: implications for the preservation of throw deficits at points of normal fault linkage. J. Struct. Geol. 31, 1145–1160.
Finch, E., Gawthorpe, R., 2017. Growth and interaction of normal faults and fault network evolution in rifts: insights from three-dimensional discrete element modelling. Geol. Soc. Lond. Spec. Publ. 439 (1), 219–248.
Fisher, Q.J., Knipe, R.J., 2001. The permeability of faults within siliciclastic petroleum reservoirs of the North Sea and Norwegian Continental Shelf. Mar. Pet. Geol. 18, 1063–1081.
Fossen, H., 2016. Structural Geology, second edition. Cambridge University Press, Cambridge.
Fossen, H., Hesthammer, J., 1997. Geometric analysis and scaling relations of deformation bands in porous sandstone. J. Struct. Geol. 19, 1479–1493.
Fossen, H., Rørnes, A., 1996. Properties of fault populations in the Gullfaks Field, northern North Sea. J. Struct. Geol. 18, 179–190.
Fossen, H., Rotevatn, A., 2016. Fault linkage and relay structures in extensional settings – a review. Earth-Sci. Rev. 154, 14–28.
Fossen, H., Johansen, S.E., Hesthammer, J., Rotevatn, A., 2005. Fault interaction in porous sandstone and implications for reservoir management; examples from southern Utah. Am. Assoc. Pet. Geol. Bull. 89, 1593–1606.
Fossen, H., Schultz, R.A., Shipton, Z.K., Mair, K., 2007. Deformation bands in sandstone – a review. J. Geol. Soc. 164, 755–769.
Fossen, H., Cavalcante, G.C.G., Pinheiro, R.V.L., Archanjo, C.J., 2019. Deformation – progressive or multiphase? J. Struct. Geol. 125, 82–99.
Færseth, R.B., 2006. Shale smear along large faults: continuity of smear and the fault seal capacity. J. Geol. Soc. 163, 741–751.
Færseth, R.B., Johnsen, E., Sperrevik, S., 2007. Methodology for risking fault seal capacity: implications of fault zone architecture. Am. Assoc. Pet. Geol. Bull. 91, 1231–1246.
Gartrell, A.P., Zhang, Y., Lisk, M., Dewhurst, D., 2004. Fault intersections as critical hydrocarbon leakage zones: integrated field study and numerical modelling of an example from the Timor Sea, Australia. Mar. Pet. Geol. 21, 1165–1179.
Grasemann, B., Martel, S., Passchier, C.W., 2005. Reverse and normal drag along a fault. J. Struct. Geol. 27, 999–1010.
Gudmundsson, A., 2011. Rock Fractures in Geological Processes. Cambridge University Press.
Gupta, A., Scholz, C.H., 2000. A model of normal fault interaction based on observations and theory. J. Struct. Geol. 22, 865–879.

Healy, D., Blenkinsop, T.G., Timms, N.E., Meredith, P.G., Mitchell, T.M., Cooke, M.L., 2015. Polymodal faulting: time for a new angle on shear failure. J. Struct. Geol. 80, 57–71.
Henza, A.A., Withjack, M.O., Schlische, R.W., 2010. Normal-fault development during two phases of non-coaxial extension: an experimental study. J. Struct. Geol. 32, 1656–1667.
Husmo, T., Hamar, G.P., Høiland, O., Johannesen, E.P., Rømuld, A., Spencer, A.M., et al., 2002. Lower and Middle Jurassic. In: Evans, D., Graham, C., Armour, A., Bathurst, P. (Eds.), The Millennium Atlas: Petroleum Geology of the Central and Northern North Sea. Geological Society, London, pp. 129–155.
Johansen, T.E.S., Fossen, H., Kluge, R., 2005. The impact of syn-kinematic porosity reduction on damage zone architecture in porous sandstone; an outcrop example from the Moab Fault, Utah. J. Struct. Geol. 27, 1469–1485.
Johri, M., Zoback, M.D., Hennings, P., 2014. A scaling law to characterize fault-damage zones at reservoir depths. AAPG Bull. 98, 2057–2079.
Kelly, P.G., Peacock, D.C.P., Sanderson, D.J., McGurk, A.C., 1999. Selective reverse-reactivation of normal faults, and deformation around reverse-reactivated faults in the Mesozoic of the Somerset coast. J. Struct. Geol. 21, 493–509.
Knipe, R.J., Fisher, Q.J., Clennell, M.R., Farmer, A.B., Harrison, A., Kidd, B., et al., 1997. Fault seal analysis: successful methodologies, application and future directions. In: Møller-Pedersen, P. & Koestler, A.G. (Eds.), Hydrocarbon Seals: Importance for Exploration and Production: Norwegian Petroleum Society Special Publication, vol. 7. Elsevier, pp. 15–40.
Krantz, R.W., 1988. Multiple fault sets and three-dimensional strain: theory and application. J. Struct. Geol. 10 (3), 225–237.
Lamarche, G., Barnes, P.M., Bull, J.M., 2006. Faulting and extension rate over the last 20,000 years in the offshore Whakatane Graben, New Zealand continental shelf. Tectonics 25. Available from: https://doi.org/10.1029/2005tc001886.
Long, J.J., Imber, J., 2011. Geological controls on fault relay zone scaling. J. Struct. Geol. 33, 1790–1800.
Maerten, L., Maerten, F., 2006. Chronologic modeling of faulted and fractured reservoirs using geomechanically based restoration: technique and industry applications. Am. Assoc. Pet. Geol. Bull. 90, 1201–1226.
Maerten, L., Gillespie, P., Pollard, D.D., 2002. Effects of local stress perturbation on secondary fault development. J. Struct. Geol. 24, 145–153.
Marrett, R., Allmendinger, R.W., 1990. Kinematic analysis of fault-slip data. J. Struct. Geol. 12, 973–986.
Marrett, R., Allmendinger, R.W., 1992. Amount of extension on "small" faults: an example from the Viking Graben. Geology 20, 47–50.
Marshak, S., Karlstrom, K.E., Timmons, J.M., 2000. Inversion of Proterozoic extensional faults: an explanation for the pattern of Laramide and Ancestral Rockies intracratonic deformation, United States. Geology 28, 735–738.
Martel, S., Pollard, D.D., Segall, P., 1988. Development of simple strike-slip fault zones, Mount Abbot quadrangle, Sierra Nevada, California. Geol. Soc. Am. Bull. 100, 1451–1465.
McGill, G.E., Stromquist, A.W., 1979. The grabens of Canyonlands National Park, Utah – geometry, mechanics, and kinematics. J. Geophys. Res. 84, 4547–4563.
Micklethwaite, S., Cox, S.F., 2004. Fault-segment rupture, aftershock-zone fluid flow, and mineralization. Geology 32 (9), 813.
Micklethwaite, S., Cox, S., 2006. Progressive fault triggering and fluid flow in aftershock domains: examples from mineralized Archaean fault systems. Earth Planet. Sci. Lett. 250 (1–2), 318–330.
Moore, J.M., Schultz, R.A., 1999. Processes of faulting in jointed rocks of Canyonlands National Park, Utah. GSA Bull. 111, 808–822.
Morellato, C., Redini, F., Doglioni, C., 2003. On the number and spacing of faults. Terra Nova 15 (5), 315–321.
Nicol, A., Gillespie, P., Childs, C., Walsh, J.J., 2002. Relay zones between mesoscopic thrust faults in layered sedimentary sequences. J. Struct. Geol. 24, 709–727.
Oertel, G., 1965. The mechanism of faulting in clay experiments. Tectonophysics 2, 343–393.
Peace, A., McCaffrey, K., Imber, J., van Hunen, J., Hobbs, R., Wilson, R., 2018. The role of pre-existing structures during rifting, continental breakup and transform system development, offshore West Greenland. Basin Res. 30 (3), 373–394.
Peacock, D.C.P., 2001. The temporal relationship between joints and faults. J. Struct. Geol. 23, 329–341.
Peacock, D.C.P., Sanderson, D.J., 1995. Strike-slip relay ramps. J. Struct. Geol. 17, 1351–1360.
Peacock, D.C.P., Sanderson, D.J., 1996. Effects of propagation rate on displacement variations along faults. J. Struct. Geol. 18, 311–320.
Peacock, D.C.P., Price, S.P., Pickles, C.S., 2000. The world's biggest relay ramp: Hold With Hope, NE Greenland. J. Struct. Geol. 22, 843–850.
Phillips, T.B., Jackson, C.A.L., Bell, R.E., Duffy, O.B., Fossen, H., 2016. Reactivation of intrabasement structures during rifting: a case study from offshore southern Norway. J. Struct. Geol. 91, 54–73.
Pollard, D.D., Fletcher, R., 2005. Fundamentals of Structural Geology. Cambridge University Press.
Ramsay, J.G., 1980. Shear zone geometry: a review. J. Struct. Geol. 2, 83–99.
Reches, Z., 1988. Evolution of fault patterns in clay experiments. Tectonophysics 145, 141–156.
Reches, Z., Lockner, D.A., 1994. Nucleation and growth of faults in brittle rocks. J. Geophys. Res. Solid Earth 99 (B9), 18159–18173.
Riedel, W., 1929. Zur Mechanik geologischer Brucherscheinungen. Cent. Miner. Geol. Paläontol. 1929 B, 354–368.
Rotevatn, A., Fossen, H., Hesthammer, J., Aas, T.E., Howell, J.A. 2007. Are relay ramps conduits for fluid flow? Structural analysis of a relay ramp in Arches National Park, Utah. In: Lonergan, L., Jolly, R.J.H., Rawnsley, K. Sanderson, D.J. (Eds.), Fractured Reservoirs, vol. 270. Geological Society, London, Special Publications, pp. 55–71.
Rowland, J.V., Sibson, R.H., 2004. Structural controls on hydrothermal flow in a segmented rift system, Taupo Volcanic Zone, New Zealand. Geofluids 4, 259–283.
Savage, H.M., Brodsky, E.E., 2011. Collateral damage: Evolution with displacement of fracture distribution and secondary fault strands in fault damage zones. J. Geophys. Res. 116, B3. Available from: https://doi.org/10.1029/2010jb007665.
Scholz, C.H., 2002. The Mechanics of Earthquakes and Faulting. Cambridge University Press, 496 pp.
Schueller, S., Braathen, A., Fossen, H., Tveranger, J., 2013. Spatial distribution of deformation bands in damage zones of extensional faults in porous sandstones: statistical analysis of field data. J. Struct. Geol. 52, 148–162.
Schultz, R.A., Soliva, R., Fossen, H., Okubo, C.H., Reeves, D.M., 2008. Dependence of displacement–length scaling relations for fractures and deformation bands on the volumetric changes across them. J. Struct. Geol. 30, 1405–1411.
Segall, P., Pollard, D.D., 1983. Joint formation in granitic rock of the Sierra Nevada. Geol. Soc. Am. Bull 94, 563–575.

Sharp, I.R., Gawthorpe, R., Underhill, J.R., Gupta, S., 2000. Fault-propagation folding in extensional settings: examples of structural style and synrift sedimentary response from the Suez Rift, Sinai, Egypt. Geol. Soc. Am. Bull. 112, 1877–1899.
Shipton, Z.K., Cowie, P., 2003. A conceptual model for the origin of fault damage zone structures in high-porosity sandstone. J. Struct. Geol. 25, 333–344.
Sibson, R.H., 1985. A note on fault reactivation. J. Struct. Geol. 7, 751–754.
Soliva, R., Benedicto, A., Maerten, L., 2006. Spacing and linkage of confined normal faults: importance of mechanical thickness. J. Geophys. Res. 111 (B1). Available from: https://doi.org/10.1029/2004jb003507.
Sperrevik, S., Gillespie, P.A., Fisher, Q.J., Halvorsen, T., Knipe, R.J., 2002. Empirical estimation of fault rock properties, Hydrocarbon Seal Quantification, 11. Elsevier, Amsterdam.
Tchalenko, J.S., 1970. Similarities between shear zones of different magnitudes. Geol. Soc. Am. Bull 81, 1625–1640.
Titus, S.J., DeMets, C., Tikoff, B., 2006. Thirty-five-year creep rates for the creeping segment of the San Andreas Fault and the effects of the 2004 Parkfield earthquake: constraints from alignment arrays, continuous global positioning system, and creepmeters. Bull. Seismol. Soc. Am. 96 (4B), S250–S268.
Trudgill, B., Cartwright, J., 1994. Relay-ramp forms and normal-fault linkages, Canyonlands National Park, Utah. Geol. Soc. Am. Bull 106, 1143–1157.
van der Zee, W., Wibberley, C.A.J., Urai, J.L., 2008. The influence of layering and pre-existing joints on the development of internal structure in normal fault zones: the Lode'ye basin, France, Geol. Soc. Lond. Spec. Publ, 299.
Vigneresse, J.L., Bouchez, J.L., 1997. Successive granitic magma batches during pluton emplacement: the case of Cabeza de Araya (Spain). J. Pet. 38, 1767–1776.
Walsh, J.J., Watterson, J., 1992. Populations of faults and fault displacements and their effects on estimates of fault-related regional extension. J. Struct. Geol. 14, 701–712.
Walsh, J.J., Bailey, W.R., Childs, C., Nicol, A., Bonson, C.G., 2003. Formation of segmented normal faults: a 3-D perspective. J. Struct. Geol. 25 (8), 1251–1262.
White, S.H., Bretan, P.G., Rutter, E.H., 1986. Fault-zone reactivation: kinematics and mechanisms. Phil. Trans. R. Soc. Lond 317, 81–97.
Wibberley, C.A.J., Shipton, Z.K., 2010. Fault zones: a complex issue. J. Struct. Geol. 32, 1554–1556.
Wibberley, C.A.J., Yielding, G., Di Toro, G., 2008. Recent advances in the understanding of fault zone internal structure: a review. In: Wibberley, C.A.J., Kurz, W., Imber, J., Holdsworth, R.E., Collettini, C. (Eds.), The Internal Structure of Fault Zones: Implications for Mechanical and Fluid-flow Properties, 299. Geological Society, London, Special Publications, pp. 5–33.
Wilkins, S.J., Gross, M.R., Wacker, M., Eydal, Y., Engelder, T., 2001. Faulted joints: kinematics, displacement-length scaling relations and criteria for their identification. J. Struct. Geol. 23, 315–327.
Woodcock, N.H., Fisher, M., 1986. Strike-slip duplexes. J. Struct. Geol. 7, 725–735.
Zuluaga, L.F., Fossen, H., Rotevatn, A., 2014. Progressive evolution of deformation band populations during Laramide fault-propagation folding: Navajo Sandstone, San Rafael monocline, Utah, U.S.A. J. Struct. Geol. 68, 66–81.